BIDIMENSIONAL EXPLORATION OF THE WARM-TEMPERATURE IONISED GAS (BETIS)

II. REVISITING THE IONISATION MECHANISM OF THE EXTRAPLANAR DIFFUSE IONISED GAS

ДВУМЕРНОЕ ИССЛЕДОВАНИЕ ТЕПЛОГО ИОНИЗОВАННОГО ГАЗА (BETIS)

II. ПЕРЕСМОТР МЕХАНИЗМОВ ИОНИЗАЦИИ ВНЕПЛОСКОСТНОГО ДИФФУЗНОГО ИОНИЗОВАННОГО ГАЗА

https://doi.org/10.1051/0004-6361/202451240

arXiv:2406.17123v2 (A&A)

Постникова Вера

VoLGa, 11 ноября 2024 г.

✔ **DIG** — diffuse ionized gas
eDIG — extra-planar ionized gas
WIM — warm ionized medium (= DIG в MW)

✔ Электронная температура ~ 10^4 K, на несколько тыс K выше областей H II, увеличивается с расстоянием от диска

✔ Электронная плотность ~ 0.01 – 0.1 см$^{-3}$, уменьшается с расстоянием от диска

✔ Для DIG свойственно увеличение отношений линий [N II]/Hα, [S II]/Hα, [O III]/Hβ, [O I]/Hα с увеличением расстояния от диска галактики

✔ В MW: составляет 20% объема ISM и 90% массы ионизованного водорода

✔ eDIG играет важнейшую роль в процессах обмена газом, металлами и энергией между диском и гало дисковых галактик, влияя на их эволюцию

Проблемы DIG

- Отсутствие <u>детального</u> исследования структуры eDIG с высоким разрешением для какой-л. выборки галактик

- Механизмы для вброса и поддержания присутствия газа на больших высотах (идея о внешних источниках провалилась, т.к. поведение DIG не скореллировано с возможными источниками извне) — ?

- Механизмы, способные обеспечить наблюдаемую степень ионизации газа — ?

- Необходимость учитывать HOLMES (hot low mass evolved stars), помимо OB-звезд — ?

  - HOLMES обладают меньшими ионизирующими светимостями, чем OB-звезды, но их число намного больше, тем более на больших высотах над плоскостью (т.к. OB-звезды сосредоточены в диске, а HOLMES распределены более равномерно по толстому диску и звездному гало)

Astronomy & Astrophysics

Bidimensional Exploration of the warm-Temperature Ionised gaS (BETIS)

II. Revisiting the ionisation mechanism of the extraplanar diffuse ionised gas

R. González-Díaz[1,2,3,*]⬤, F. F. Rosales-Ortega[2]⬤, and L. Galbany[1,3]⬤

[1] Institute of Space Sciences (ICE-CSIC), Campus UAB, Carrer de Can Magrans, s/n, E-08193 Barcelona, Spain
[2] Instituto Nacional de Astrofísica, Óptica y Electrónica (INAOE-CONAHCyT), Luis E. Erro 1, 72840 Tonantzintla, Puebla, Mexico
[3] Institut d'Estudis Espacials de Catalunya (IEEC), 08860 Castelldefels, Barcelona, Spain

ABSTRACT

The extraplanar diffuse ionised gas (eDIG) is a key component for understanding the feedback processes that connect galactic discs and their halos. In this paper, we present the second study of the Bidimensional Exploration of the warm-Temperature Ionised Gas (BETIS) project, the aim of which is to explore the possible ionisation mechanisms and characteristics of the eDIG. We use a sample of eight edge-on galaxies observed with the Multi-Unit Spectroscopic Explorer (MUSE) integral field spectrograph (IFS) and apply the methodology developed in the first paper of the BETIS project for obtaining binned emission line maps. We find that the vertical and radial profiles of the [N II]/Hα, [S II]/Hα, [O III]/Hβ, and [O I]/Hα ratios depict a complex ionisation structure within galactic halos – which is influenced by the spatial distribution of H II regions across the galactic plane as observed from our line of sight–, with Lyman continuum photon leakage from OB associations constituting the main ionisation source. Moreover, the electron temperature and S⁺/S ionisation ratio also exhibit a dependency on the distribution of H II regions within the galactic discs. Our analysis excludes low-mass, hot, and evolved stars (HOLMES) as viable candidates for secondary ionisation sources to elucidate the unusual behaviour of the line ratios at greater distances from the galactic midplane. In contrast, we ascertain that shocks induced in the interstellar medium by star formation(SF)-related feedback mechanisms represent a promising secondary ionisation source of the eDIG. We present a suite of models integrating ionisation mechanisms arising from fast shocks and photoionisation associated with star formation. When applied to the classical Baldwin–Phillips–Terlevich (BPT) diagrams, these models reveal that the ionisation budget of the eDIG ranges from 20% to 50% across our sample, with local variations of up to 20% within individual galaxy halos. This contribution correlates with the presence of filaments and other structural components observed within galaxy halos. The presence of shocks is additionally supported by the observation of a high density of high [O I]/Hα ratios, which is characteristic of shock-compressed ionised gas, and is likely induced by feedback from regions of intense SF within the galactic disc. These results demonstrate consistency across all galaxies analysed in this sample.

Key words. ISM: general – HII regions – ISM: structure – galaxies: ISM – galaxies: star formation

Исследования DIG и eDIG: "Bidimensional Exploration of the warm-Temperature Ionised gaS (BETIS) II. Revisiting the ionisation mechanism of the extraplanar diffuse ionised gas", González-Díaz et al. 2024, https://doi.org/10.1051/0004-6361/202451240

✔ 2D-анализ eDIG с высоким разрешением (FWHM < 200 пк) с помощью выборки 8 edge-on (i > 75°) галактик MUSE (z < 0.01) с низкими SFR и высокими sSFR совместно с моделями фотоионизации и ударной ионизации, ассоциированных со звездообразованием

★ Главный источник ионизации eDIG — утечка фотонов из OB-ассоциаций

★ Исключают HOLMES из возможных кандидатов на дополнительный источник ионизации eDIG

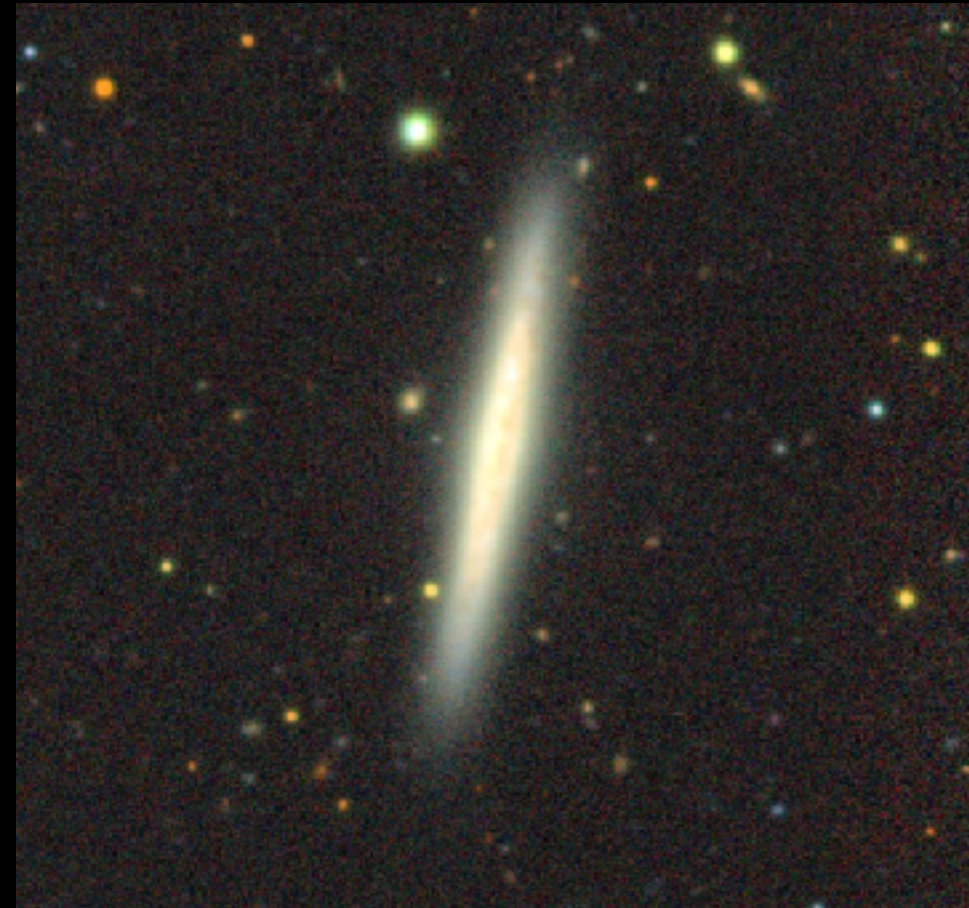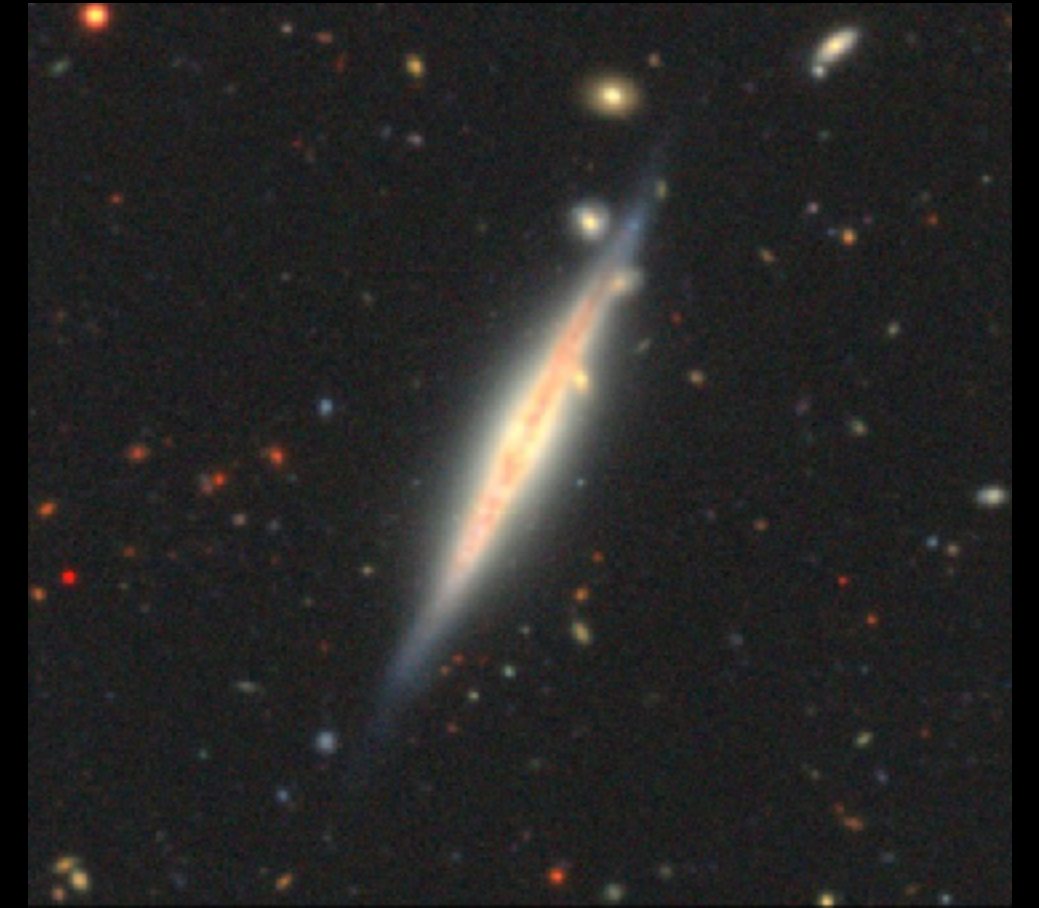★ Дополнительный источник ионизации eDIG — ударные волны как фидбек звездообразования
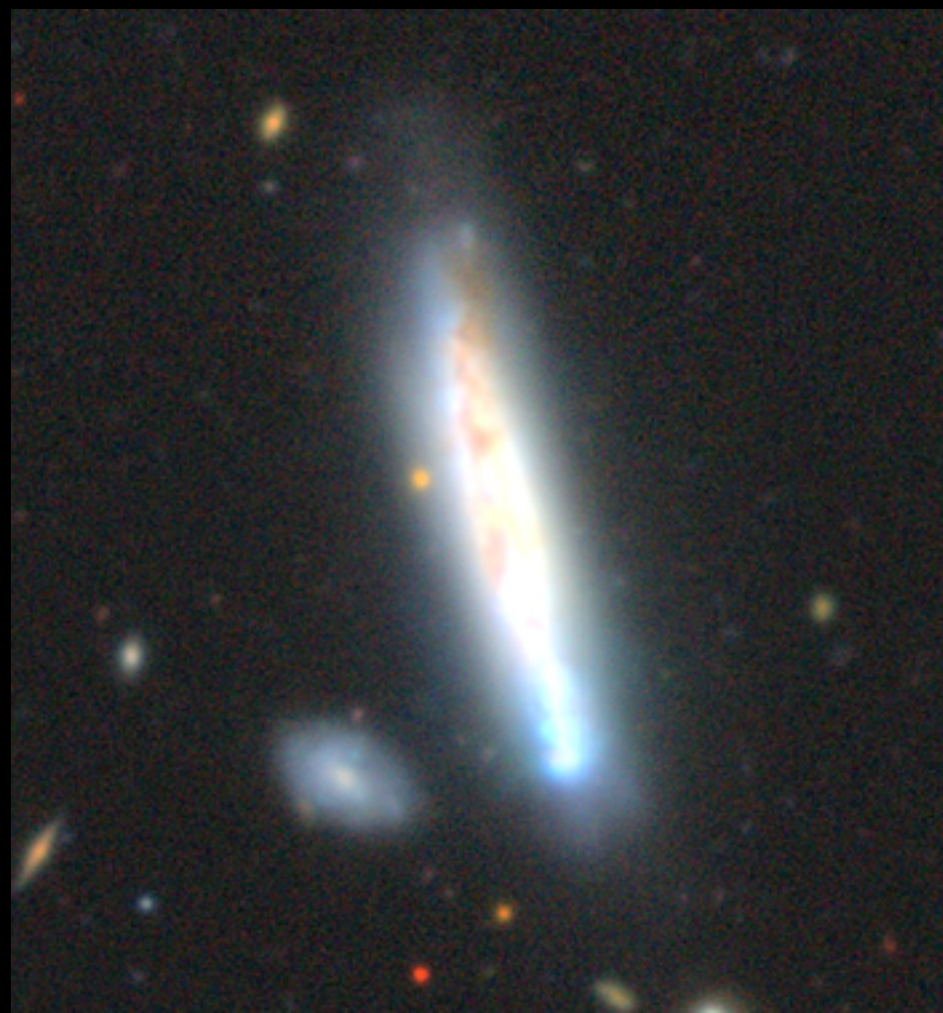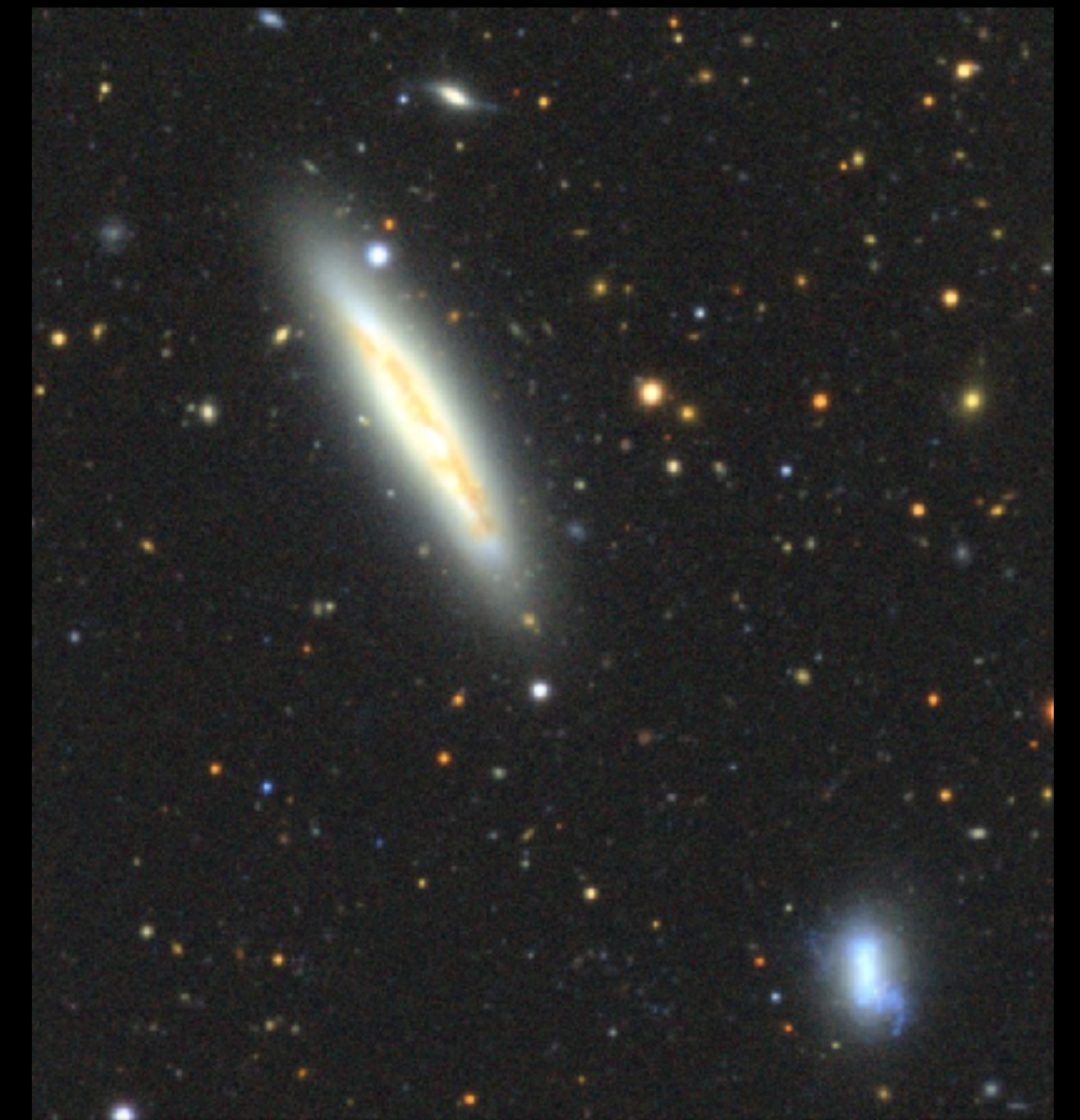
IC217　　　PGC28308　　　PGC30591　　　ESO544-27

IC1553　　　ESO443-21　　　ESO469-15　　　ESO157-49

Legacy Surveys DR9, DR10 (масштаб не сохранен)

Данные и методы

The MUSE instrument brings 1 arcmin² of field of view (FoV), with a spatial and spectral sampling of 0.2×0.2 arcsec and 1.25 Å respectively within a spectral range of 4650–9300 Å. Every datacube consists in four exposures (three for IC217) of 2624 s, and at least half of the galaxy is covered by one VLT pointing (from the centre to one of the edges of the galaxy, i.e. $0.5R_{25} < 1$ arcmin). The data was originally reduced

To conduct this exploration, we first extract the emission line features of the eBETIS sample in the form of binned emission line maps, following the same procedure described in BETIS I[2]: we employ our own adaptive binning algorithm to the original datacubes, setting a S/N target of 10 based on [S II], since this line is one of its main features of the eDIG and DIG in general, as well as it typically exhibits low S/N in both planar DIG and eDIG. Subsequently, we perform a simple stellar popula-

Данные и методы

$$\log(\text{SFR}) = \log(L_{\text{H}\alpha}) - 41.27,$$

decrement $\text{H}\alpha/\text{H}\beta = 2.87$. The galaxies are then normal-disc galaxies with low star formation. This is consistent with the clas-

grammes. Table 1 shows the integrated star formation rate (SFR) in the disc spans between $0.024\,\text{M}_\odot/\text{yr} < \text{SFR} < 0.229\,\text{M}_\odot/\text{yr}$.

with specific SFR ranging between $-10.5 < \log(\text{sSFR}/\text{yr}) < -9.92$, corresponding barely to star-forming galaxies (using MUSE data and $3.6\,\mu\text{m}$ stellar masses; Muñoz-Mateos et al.

При таком методе определения SFR странно делать вывод, что галактики имеют низкий SFR в абсолютном смысле

8

Данные и методы

$$\log(SFR) = \log(L_{H\alpha}) - 41.27,$$

decrement $H\alpha/H\beta = 2.87$. The galaxies are then normal-disc galaxies with low star formation. This is consistent with the clas-

grammes. Table 1 shows the integrated star formation rate (SFR) in the disc spans between $0.024\,M_\odot/yr < SFR < 0.229\,M_\odot/yr$.

with specific SFR ranging between $-10.5 < \log(sSFR/yr) < -9.92$, corresponding barely to star-forming galaxies (using MUSE data and $3.6\,\mu m$ stellar masses; Muñoz-Mateos et al.

Table 1. General characteristics of the eBETIS sample, in order of declination.

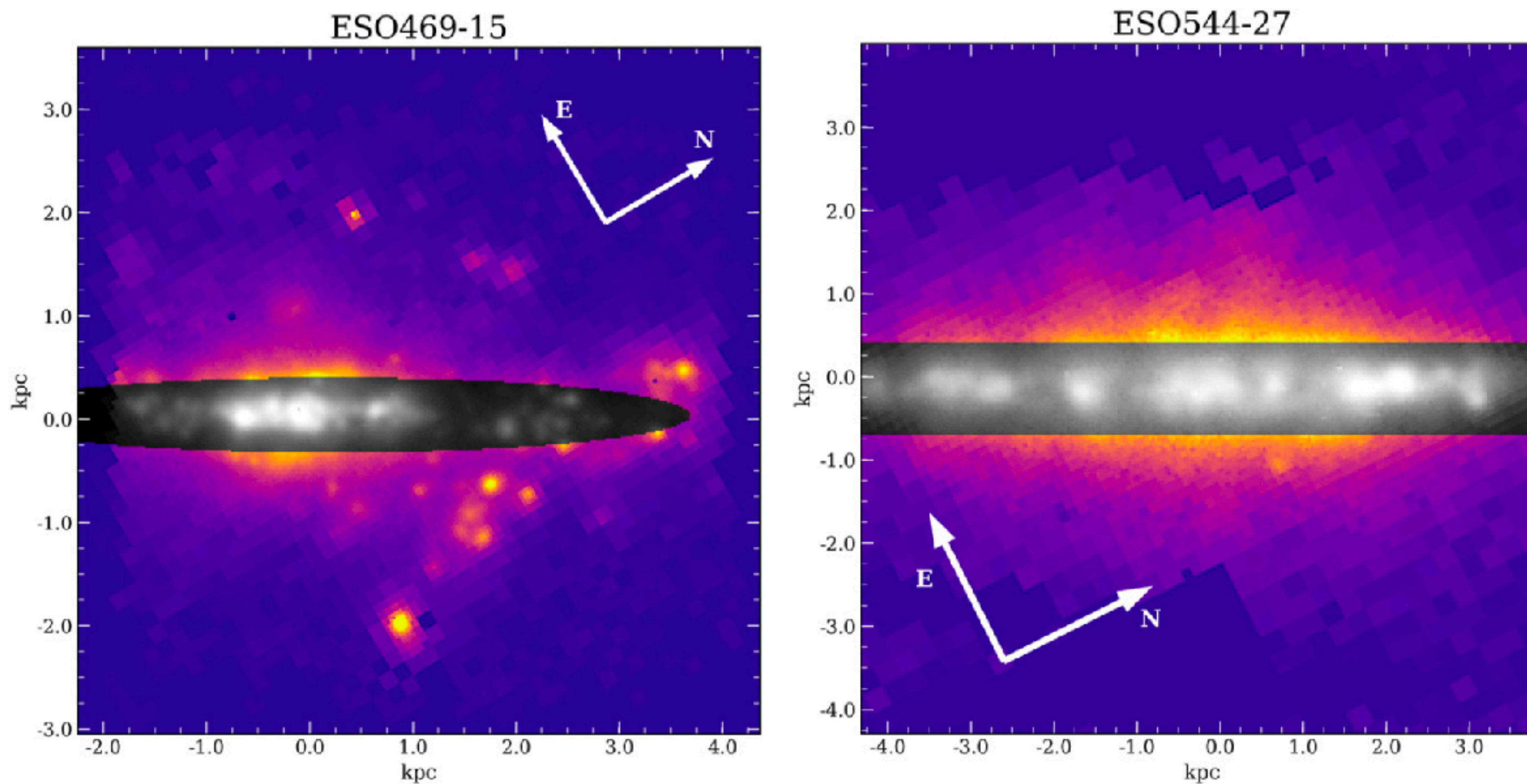| Galaxy	RA (J2000) (deg)	Dec (J2000) (deg)	Type	z	D (Mpc)	PA (°)	FWHM (pc)	Incl. (°)	log SB lim. (erg/s/kpc^2)	Bin size (pc)	$L_{eDIG}(H\alpha)$ (erg/s)	log SFR$_{Disc}$ (M$_\odot$/yr)
IC217	34.0435	−11.9267	Scd	0.00630	24.32	35.7	117.91	82.6	35.6	94.3	39.11	0.063
PGC28308	147.5582	−12.0576	Scd	0.00907	45.22	125.2	153.46	85.5	35.2	175.4	39.12	0.084
PGC30591	156.3603	−15.3492	Sd	0.00676	35.22	169.2	187.83	86.6	36.0	136.6	39.13	0.055
ESO544-27	33.2277	−19.3168	Sb	0.00818	32.81	153.3	159.07	90.0	35.0	127.2	38.92	0.024
IC1553	8.1671	−25.6075	Irr	0.00979	32.25	15.0	171.99	78.6	36.5	125.1	39.80	0.229
ESO443-21	194.9412	−29.6002	Scd	0.00941	40.31	160.8	195.45	79.0	36.6	156.4	39.71	0.184
ESO469-15	347.2317	−30.8579	Sb	0.00545	19.81	149.2	86.44	90.0	35.9	76.9	38.90	0.029
ESO157-49	69.9036	−53.0126	Sc	0.00559	24.82	30.4	96.26	79.3	35.3	96.3	39.46	0.060

Notes. The columns represent, from left to right: the designation of the galaxy, the RA and Dec in the J2000 epoch, the morphological Hubble type, the redshift, the distance in Mpc, the position angle (in deg), the PSF FWHM in pc, inclination with respect to the line of sight (in deg), the $2\sigma\,\Sigma_{H\alpha}$ limit and the average physical size of the bins in pc. The RA, Dec, the morphological type, the redshift, and distances are obtained from NED. The position angles and inclinations are obtained directly from Com19 and Hyperleda. The last columns represent the integrated $H\alpha$ luminosity within the eDIG and the integrated SFR of the disc (see Section 2).

No AGNs!

Fig. 1. eBETIS sample. The images correspond to the binned Hα emission line maps obtained in Sect. 2. Each image is rotated PA-90,° with the white arrows indicating the direction of the celestial north and east in the original image. The ellipse fitting of the galactic plane (see Sect. 2) is coloured in grey scale. The contrast between the galactic plane and the extraplanar gas reveals the complexity of the ionised extraplanar gas, which comprises diffuse gas, filaments, and various structures.

Сложная структура DIG в Hα
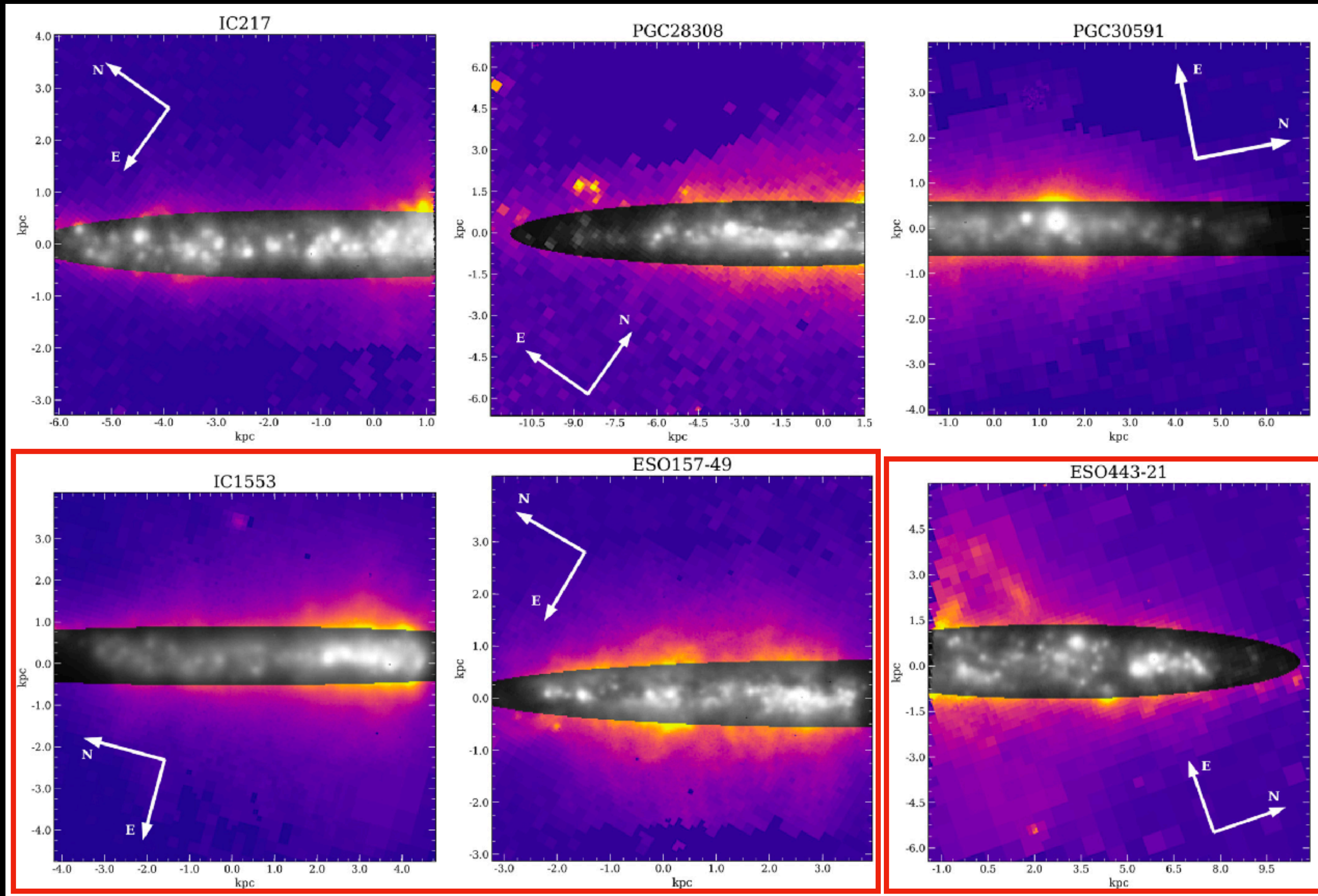
The most discernible morphological structures observed in the outer regions of the galaxy are the filaments. In galaxies such as ESO157-49 and IC1553, these filaments are especially visible, emerging from the galactic plane and extending more than 2 kpc from the midplane.

Other structures can be observed, for instance, in ESO443-21, which features a thick knot-shaped filament around the galactic centre that reaches a distance of ~4.5 kpc from the midplane.
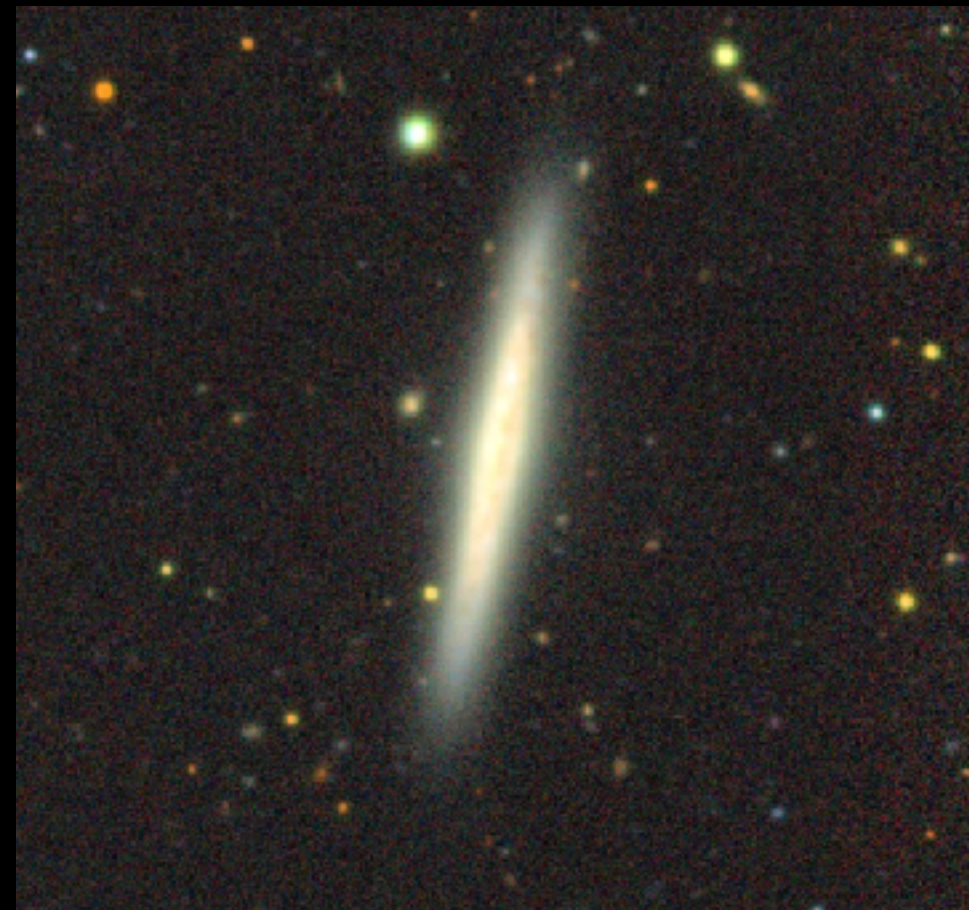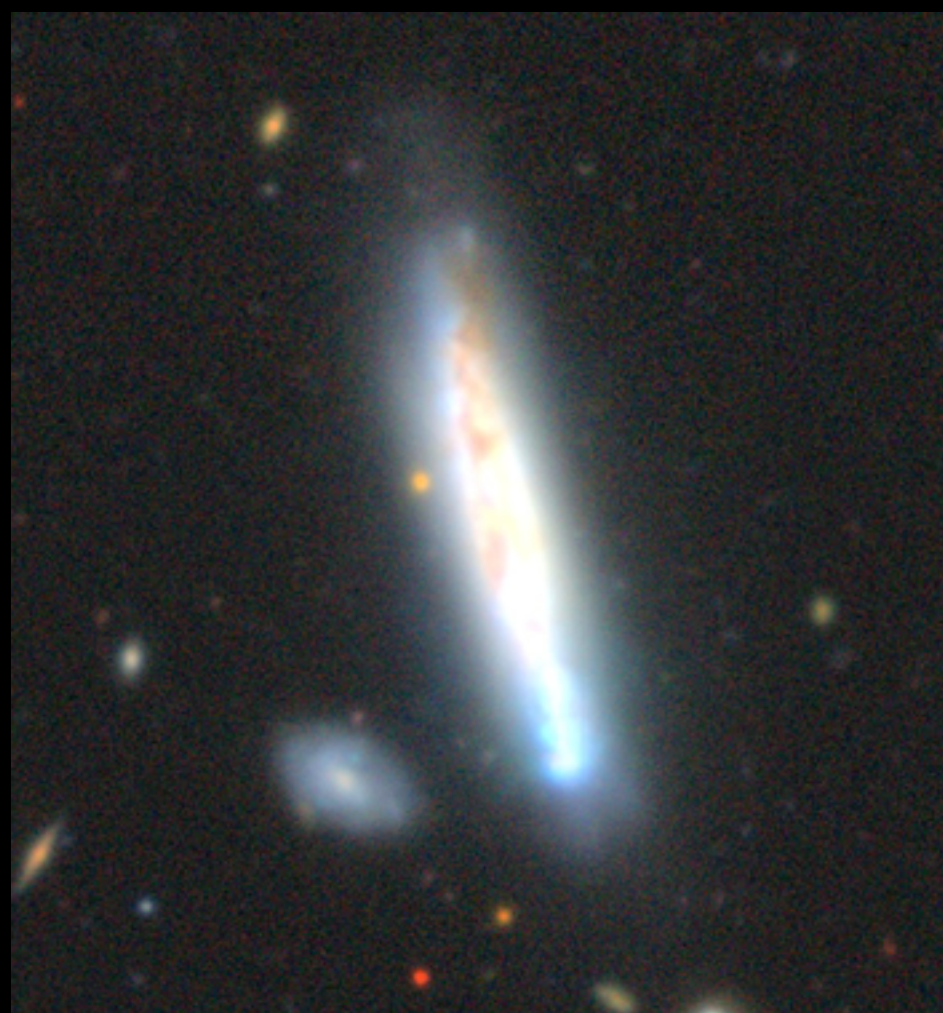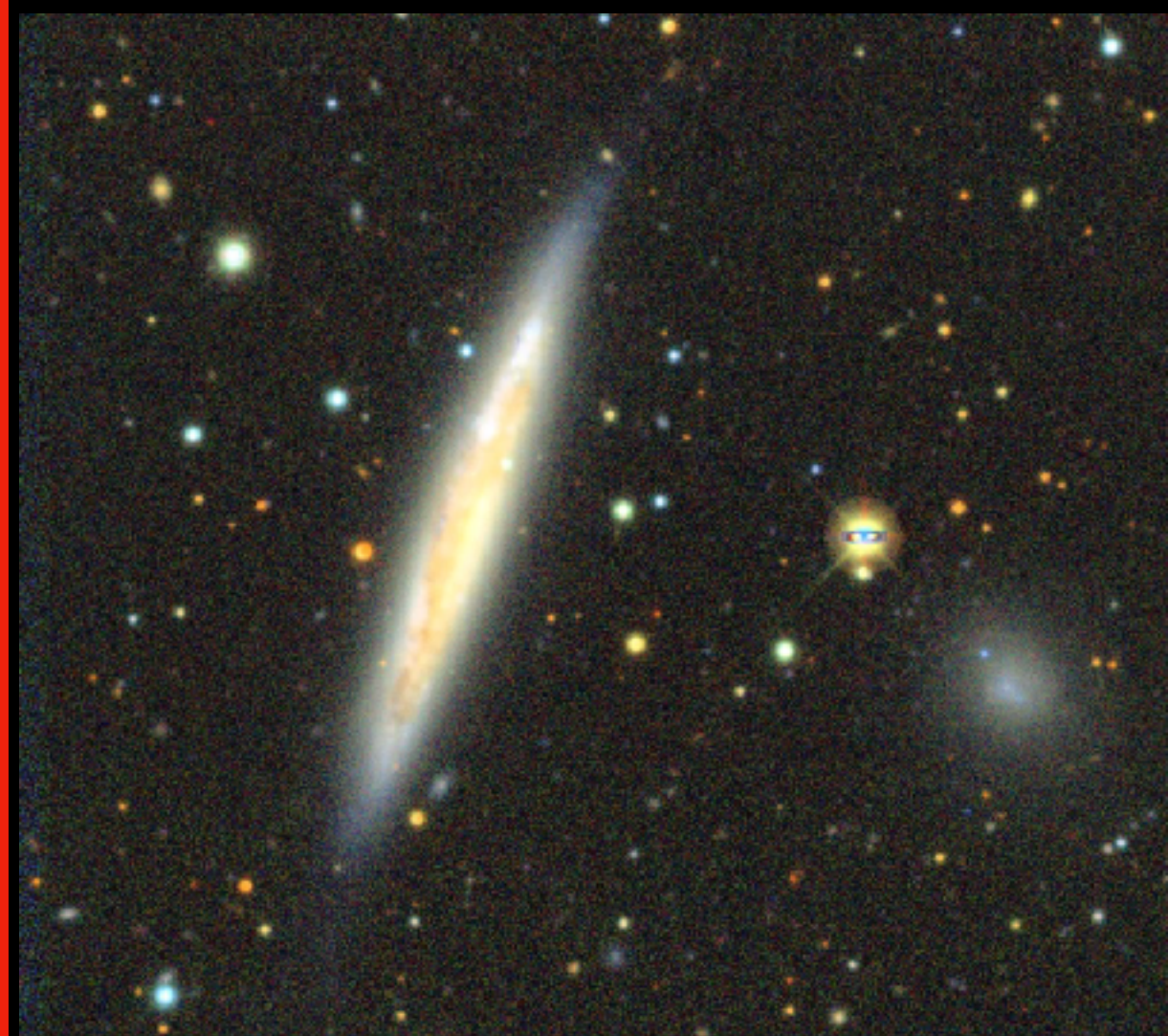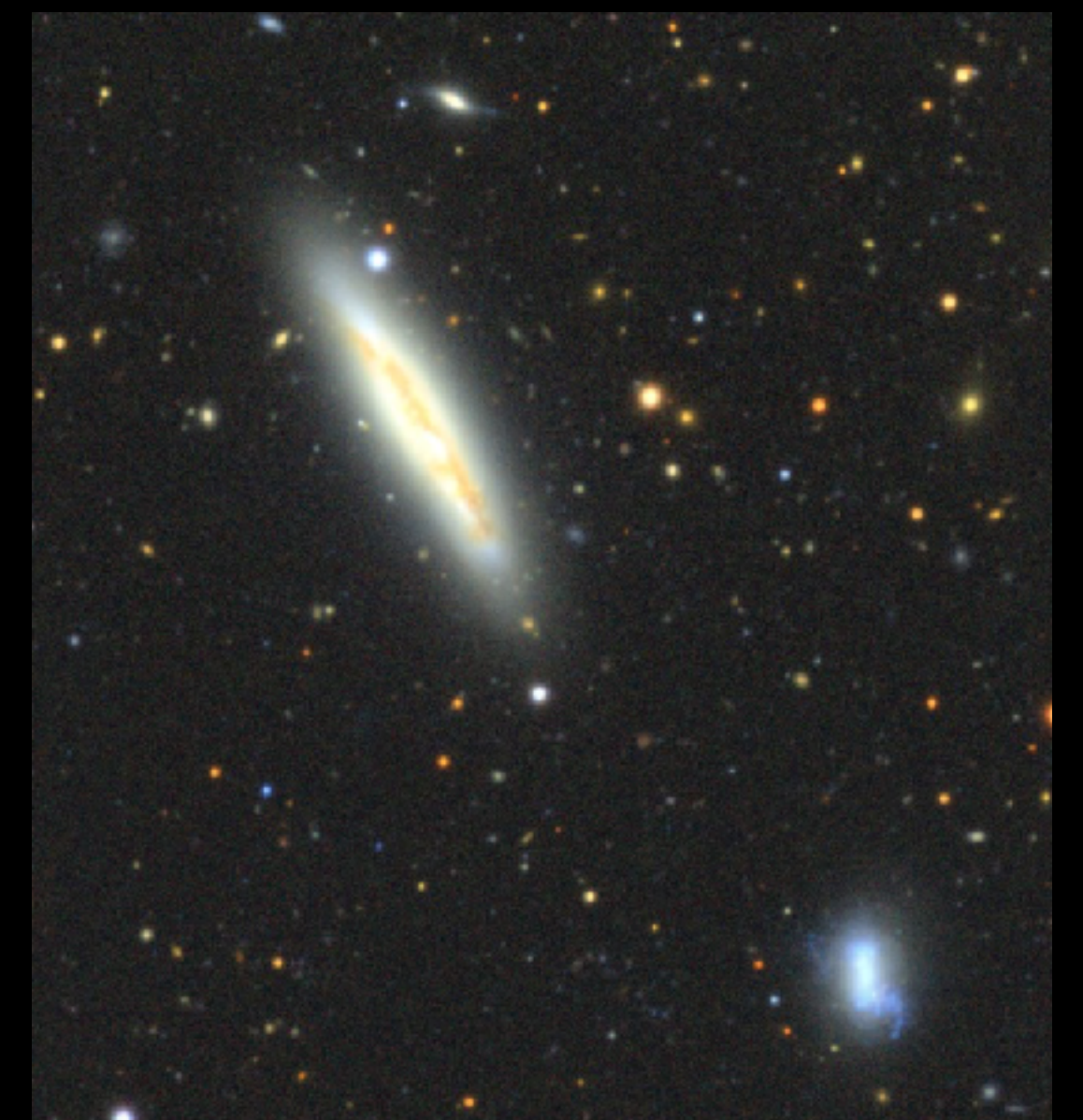
IC217   PGC28308   PGC30591   ESO544-27

IC1553   ESO443-21   ESO469-15   ESO157-49

Legacy Surveys DR9, DR10 (масштаб не сохранен)

Fig. 2: IC1553 line ratio maps. Every map is masked, excluding those bins with S/N < 2 or relative error greater than 40% for the respective lines. We overlay the same Hα map of the galactic plane masked in Figure 1. The dashed red line indicates the midplane, located at z = 0. The y-axis is re-scaled in function of the galaxy inclination.In this case, the galactic plane is defined as a rectangle with the minor side equal to the minor axis of the fitted ellipse and the major side extending the full length of the x-axis. The grey dashed lines indicates the heights with respect the midplane z = ±1, ±2, ±3 kpc and major axis distances MAD = -2.5, 0, 3 kpc.

The images show the intricate and asymmetrical structure of the eDIG. Having differences of 0.4 dex in the [S II]/Hα ratio along the major axis and over 0.8 dex in [N II]/Hα. Additionally, the line ratios increase with respect to the distance from the midplane, a phenomenon that is well-documented in the literature (Rand 1998; Levy et al. 2019). However, the 2D spectroscopic analysis of the eDIG allows to recognise that the variation of the line ratios are dependent not only on height, but along the major axis distance (MAD) of the galaxy.

[S II]/Hα, [O III]/Hβ, and [O I]/Hα maps, revealing the presence of new structures, such as an apparent biconical structure in IC1553 or a broad ionised knot in ESO443-21. The behaviour of
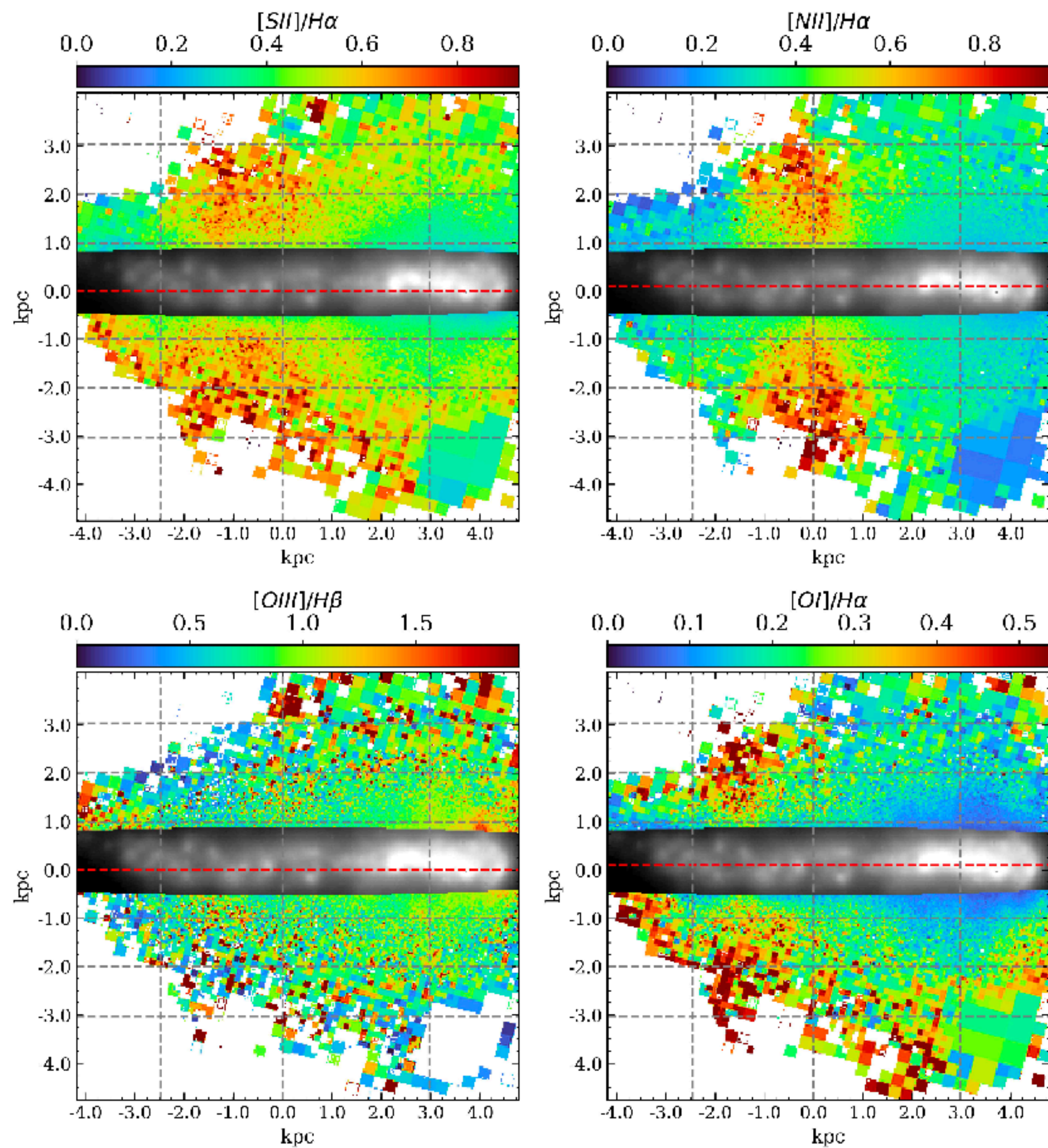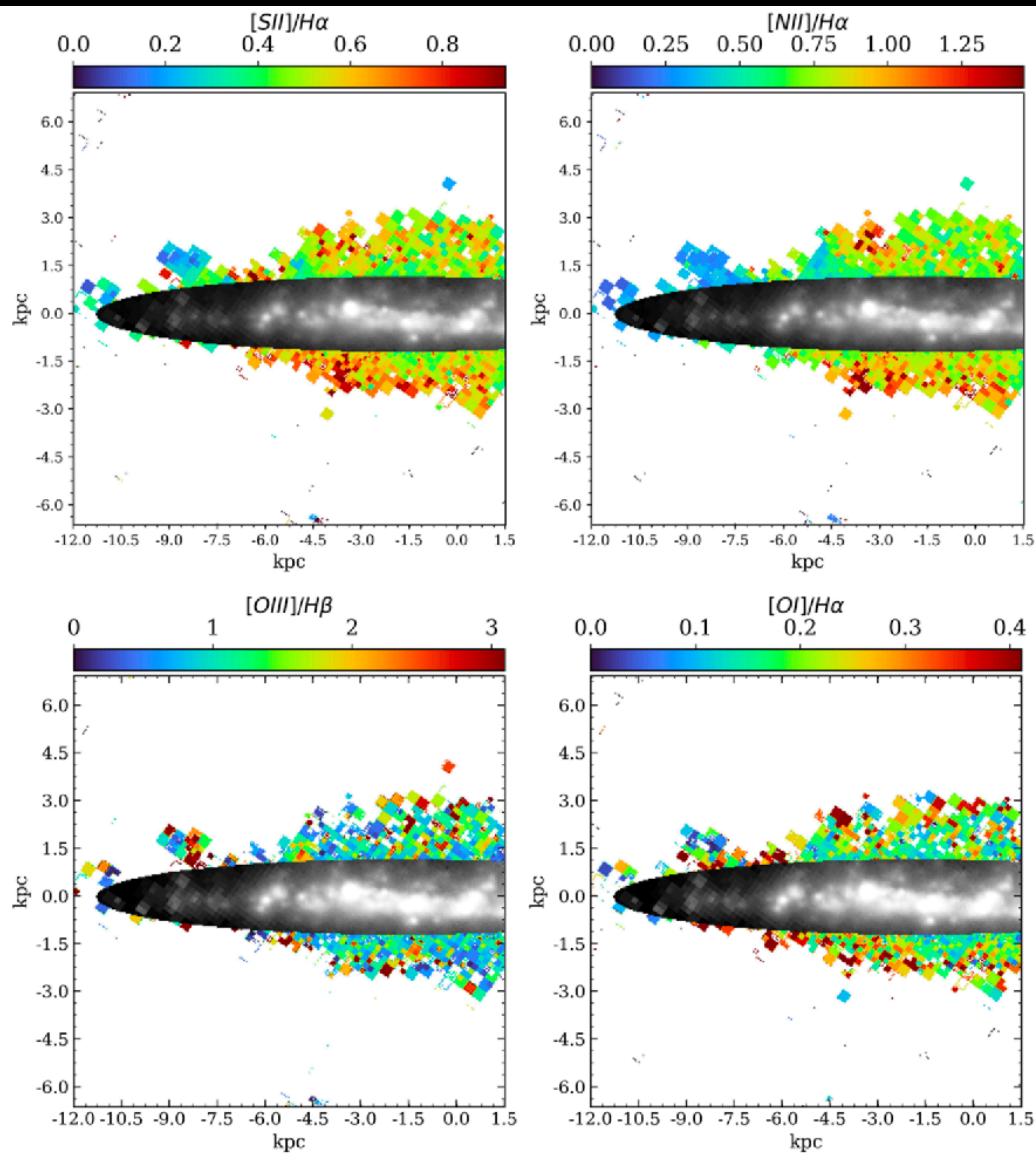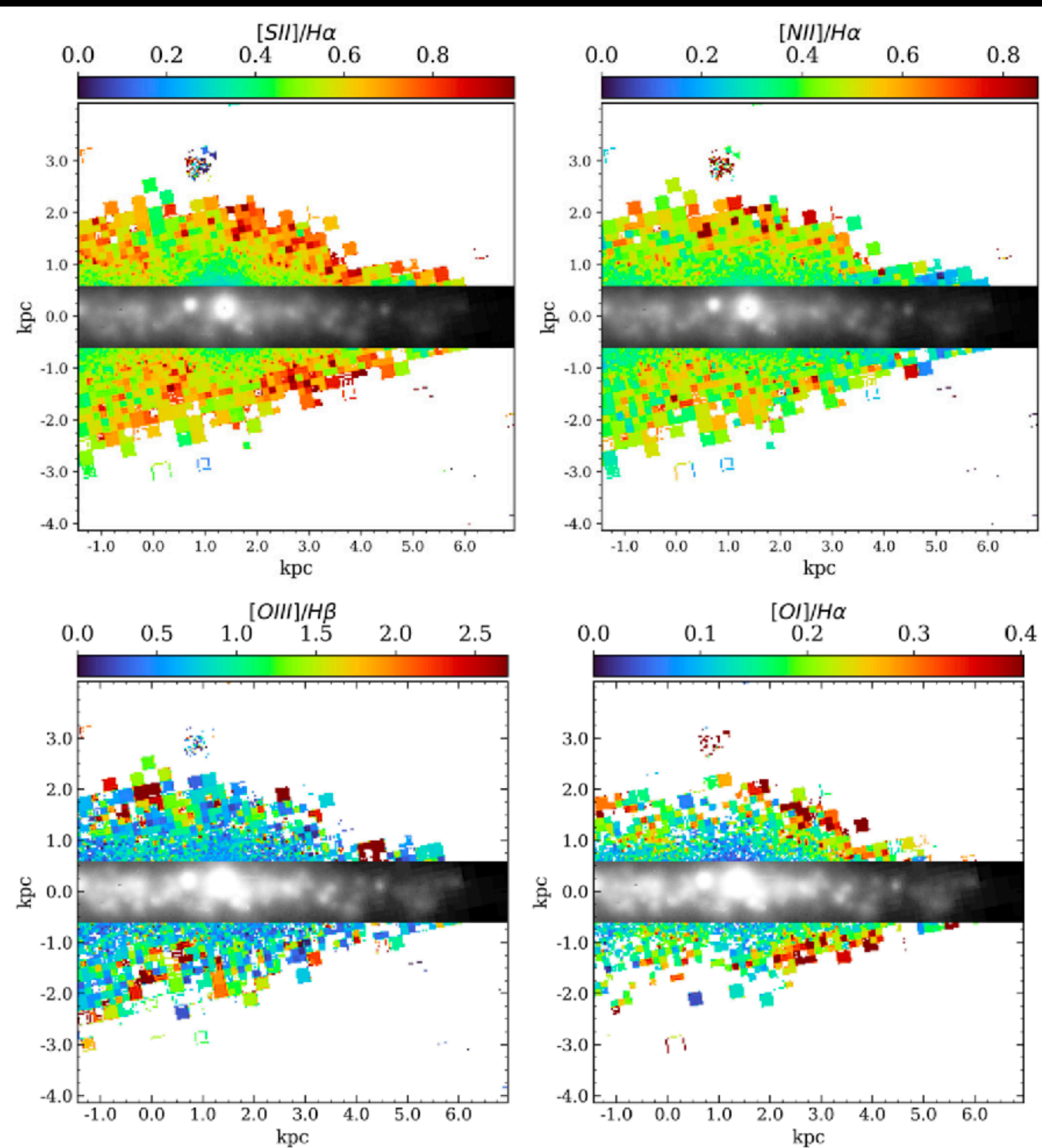

IC1553

Fig. A.1. PGC28308 line ratio maps, similar to Figure 2.
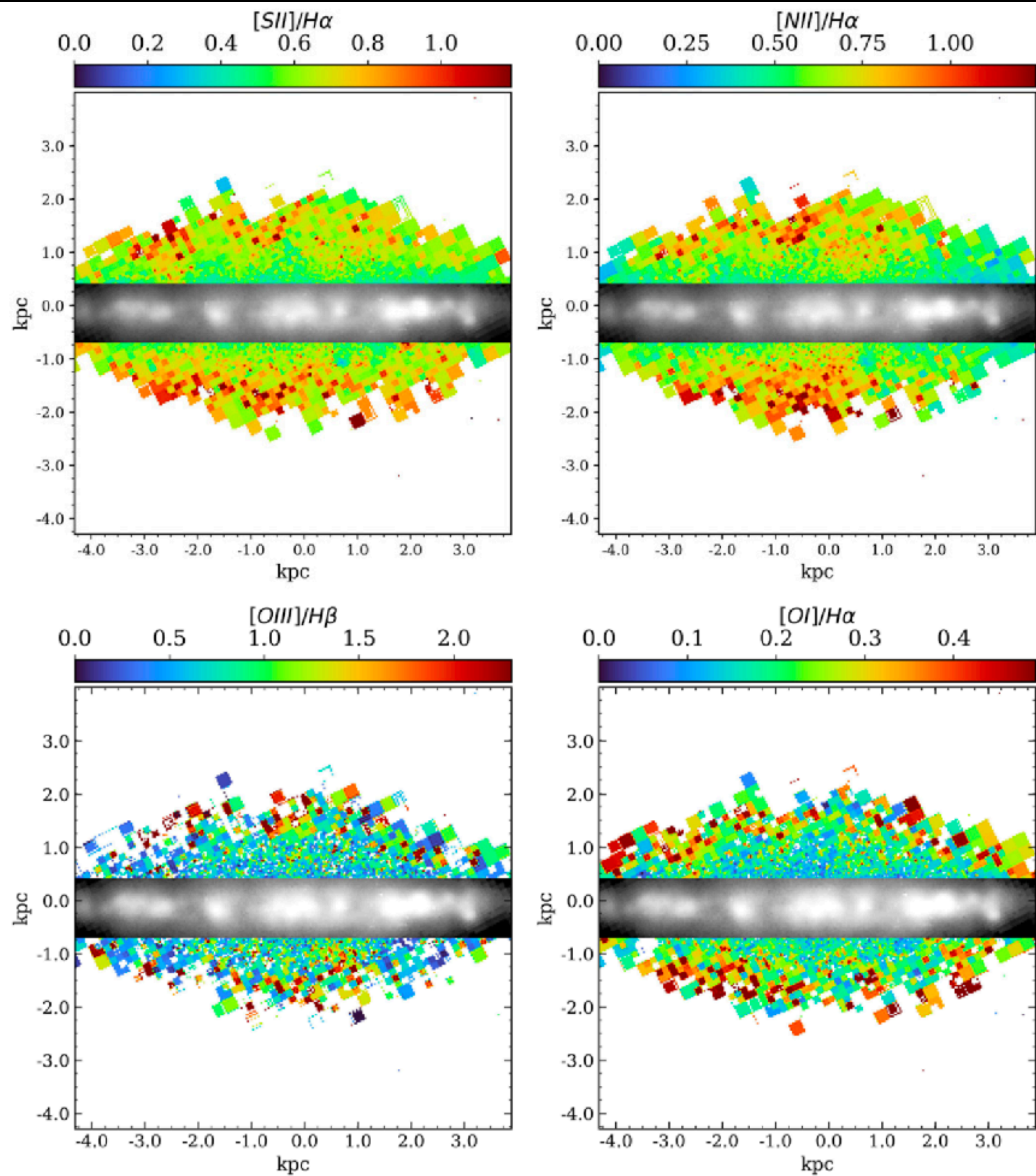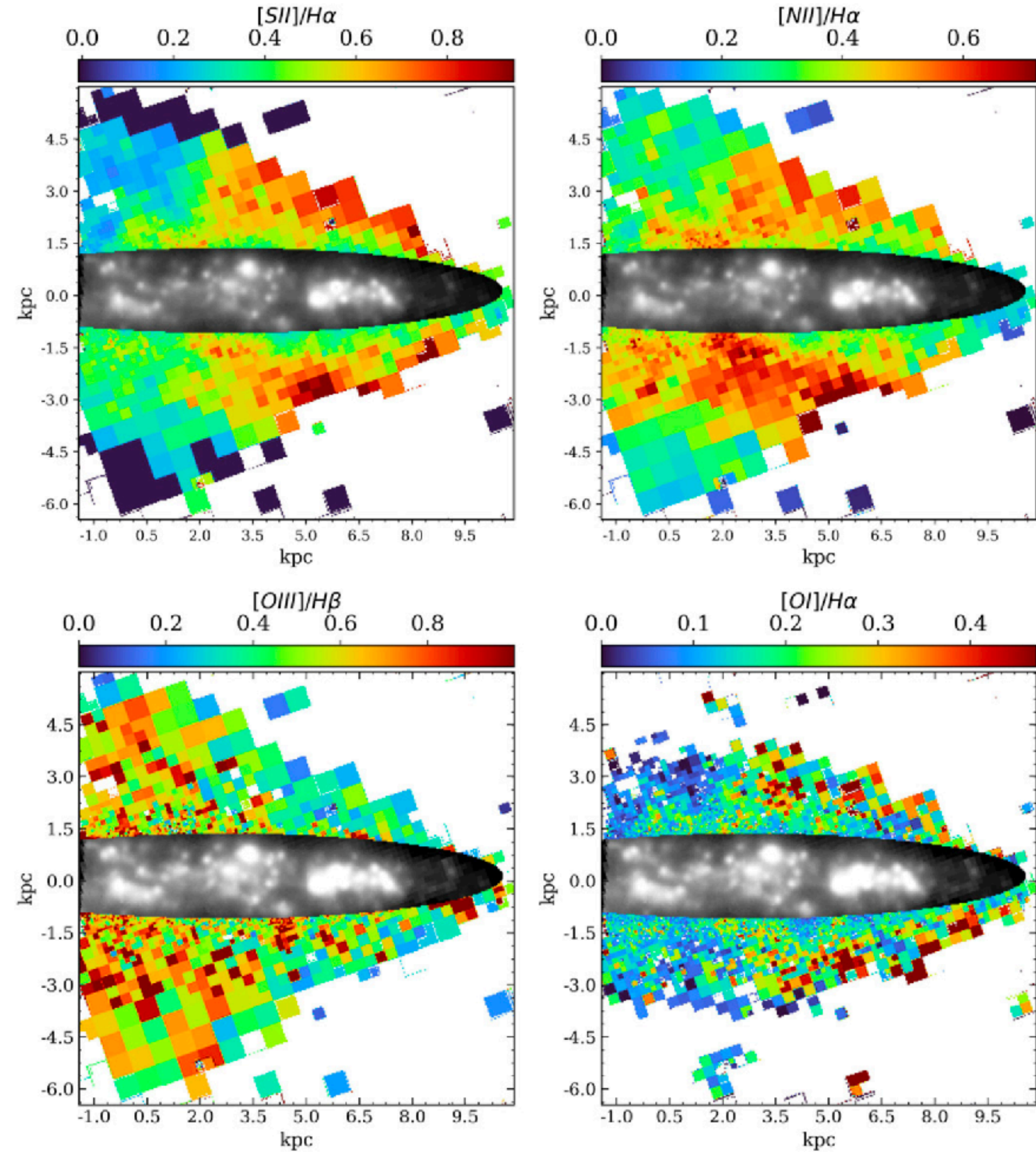
Fig. B.1. PGC30591 line ratio maps, similar to Figure 2.
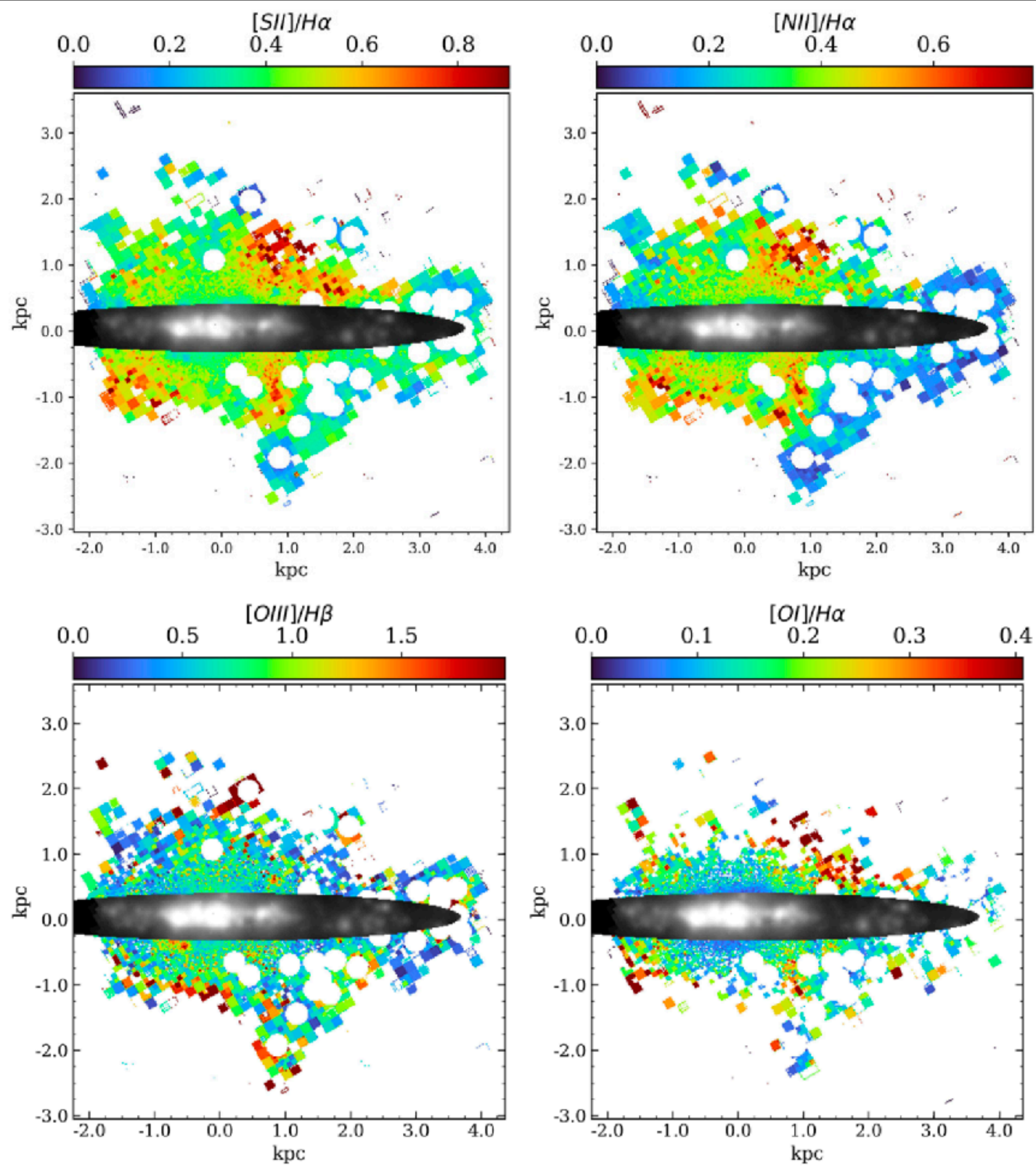
Fig. C.1. ESO544-27 line ratio maps, similar to Figure 2.
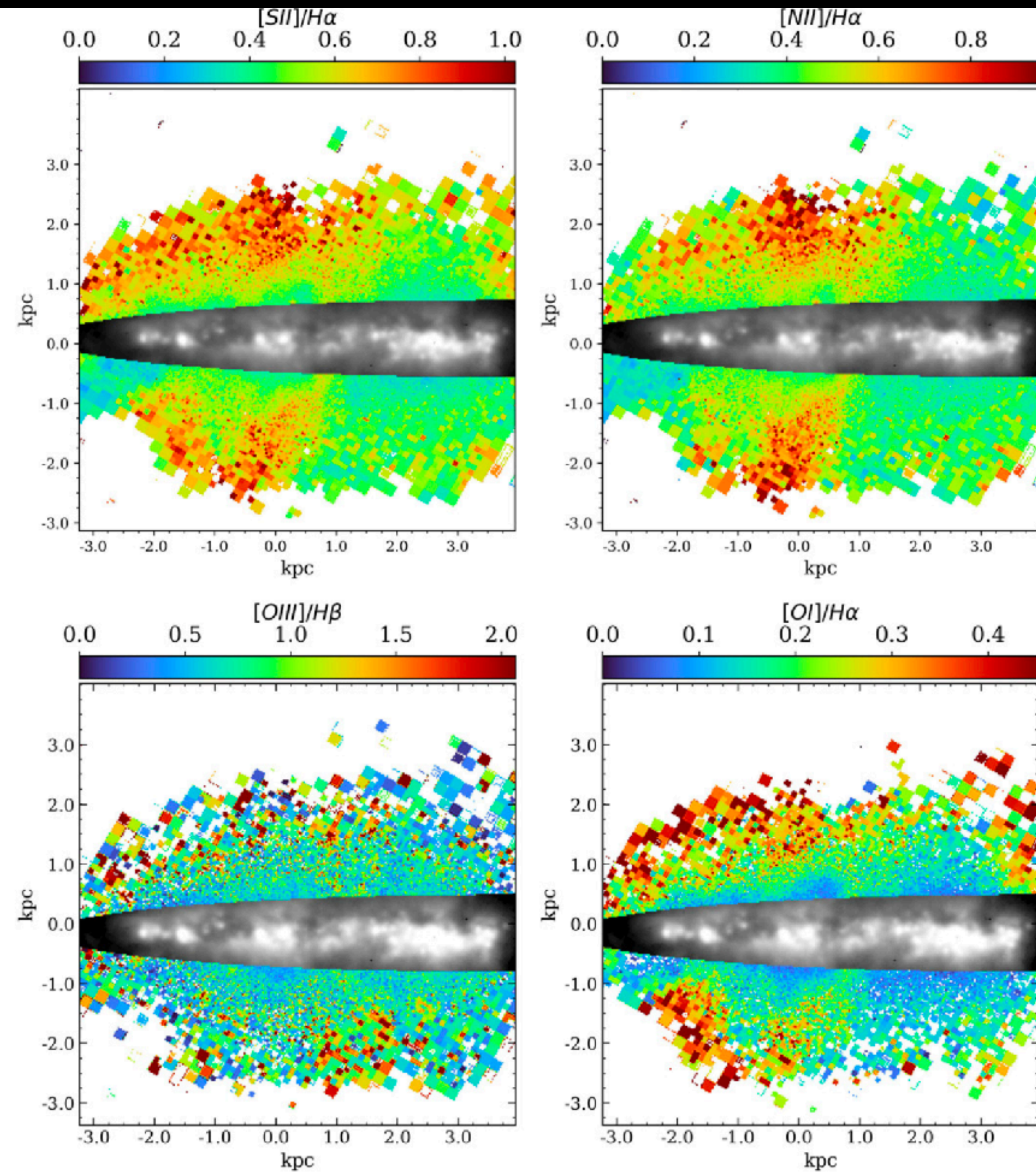
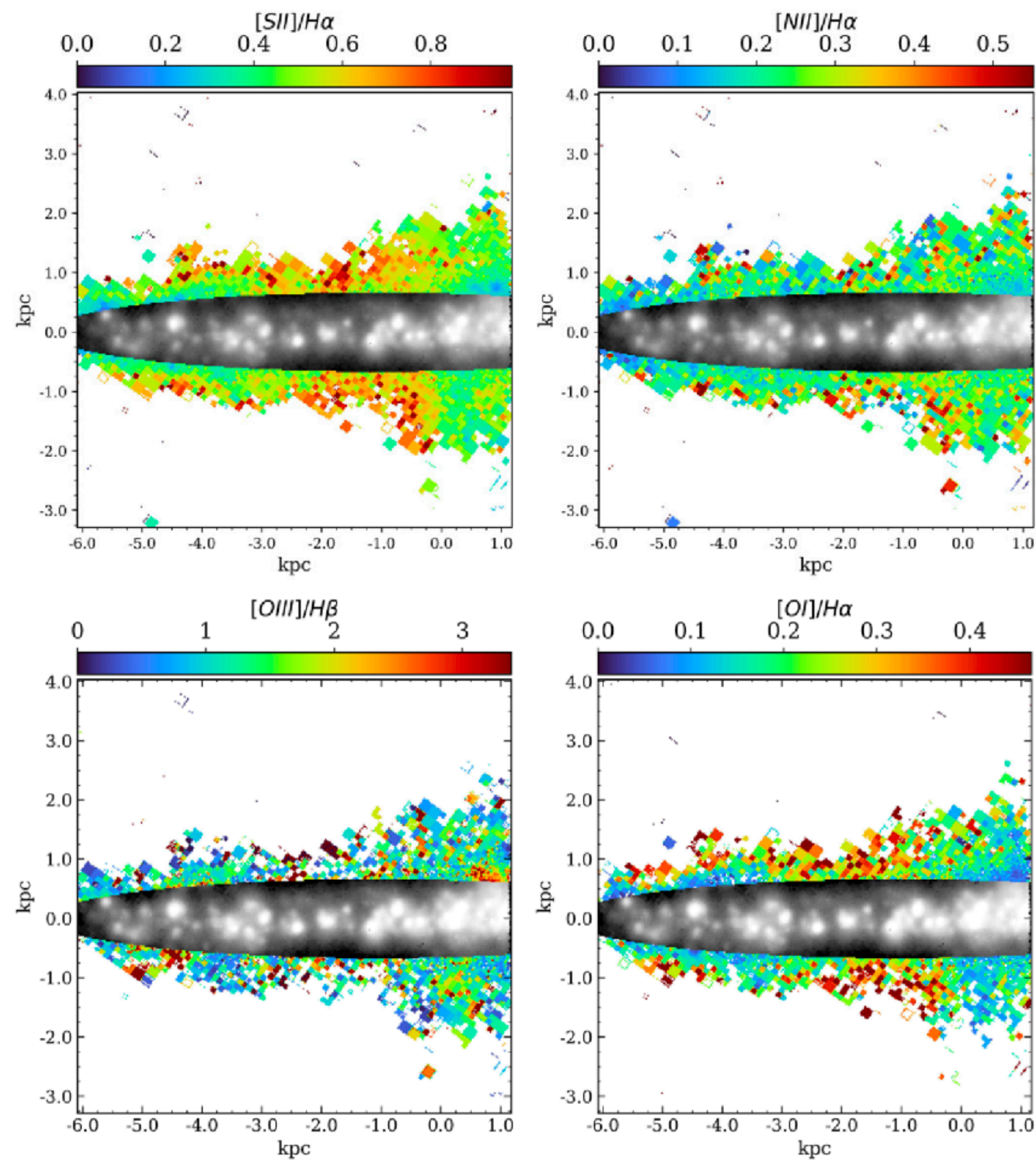**Fig. D.1.** ESO443-21 line ratio maps, similar to Figure 2.

Fig. E.1. ESO469-15 line ratio maps, similar to Figure 2.

**Fig. F.1.** ESO157-49 line ratio maps, similar to Figure 2.

Fig. G.1. IC217 line ratio maps, similar to Figure 2.

Table 2. Summary of characteristics of the eDIG.

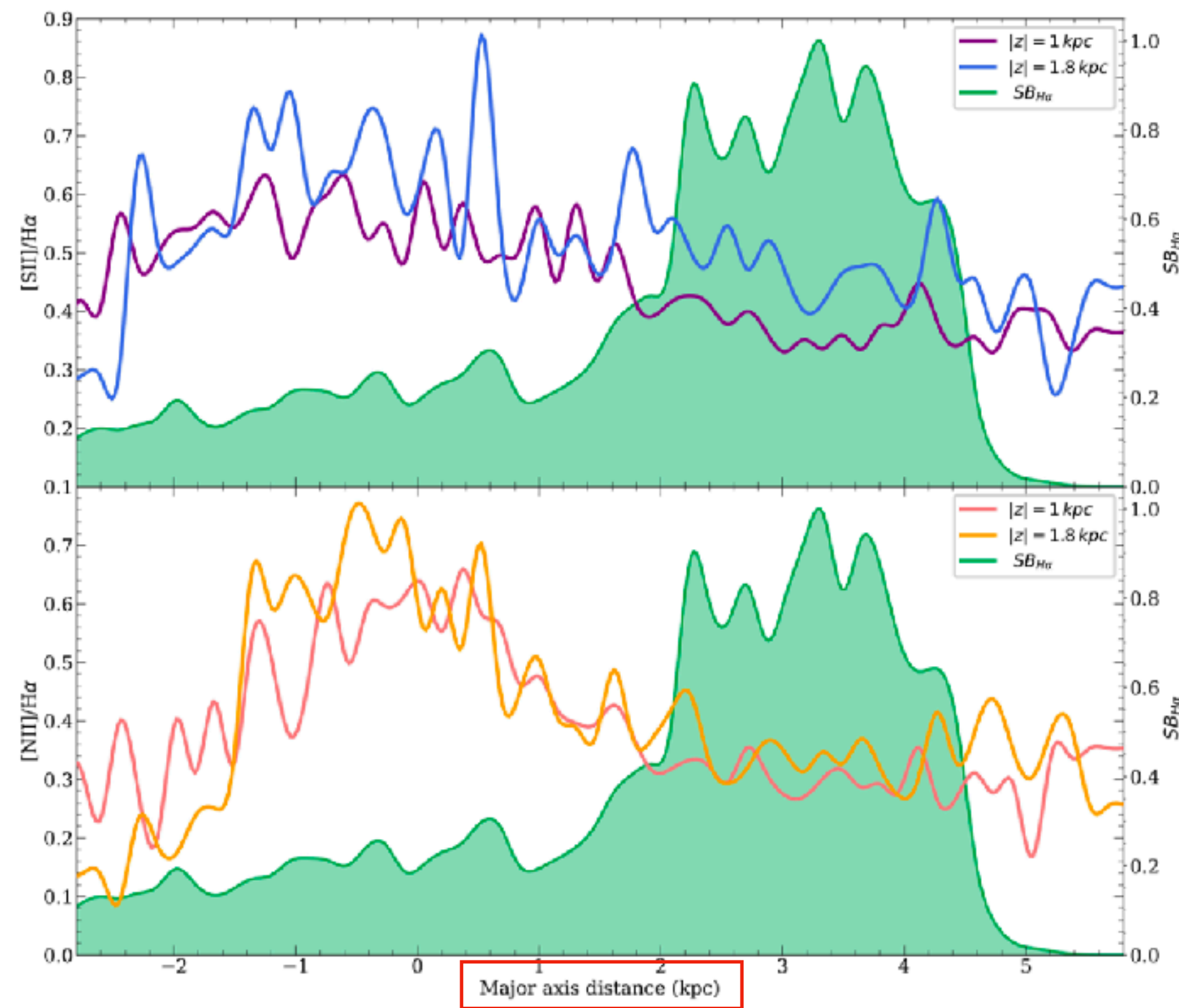| Galaxy	DIG morphology	MAD, z (kpc)
IC217	Disc: Homogeneous distribution of bright H II regions	
	Halo: Thin eDIG layer, low S/N	6, 2
PGC28308	Disc: Homogeneous distribution of bright H II regions	
	Halo: Extended and homogeneous eDIG	8, 2
PGC30591	Disc: Few bright H II regions	
	Halo: Inhomogeneous extended eDIG	4, 2
ESO544-27	Disc: Homogeneous distribution of bright H II regions	
	Halo: Homogeneous eDIG and extended filaments	4, 2
IC1553	Disc: Inhomogeneous distribution of H II regions with respect the line of sight, hidden H II regions	
	Halo: Highly asymmetrical eDIG structure with a bicone and extended filaments	4, 3.5
ESO443-21	Disc: Homogeneous distribution of bright H II regions	
	Halo: Extended eDIG with a large filamentary knot	8, 5
ESO469-15	Disc: Bright emission around the centre	
	Halo: Several extraplanar H II regions, mixed eDIG regimes	3, 2
ESO157-49	Disc: Homogeneous distribution of bright H II regions	
	Halo: Tilted and mixed eDIG regimes with extended filaments	4, 2.5

Notes. The second column represents the DIG morphology observed in the disc and halo from the Hα images. The third column shows the horizontal and vertical distances covered by the eDIG.
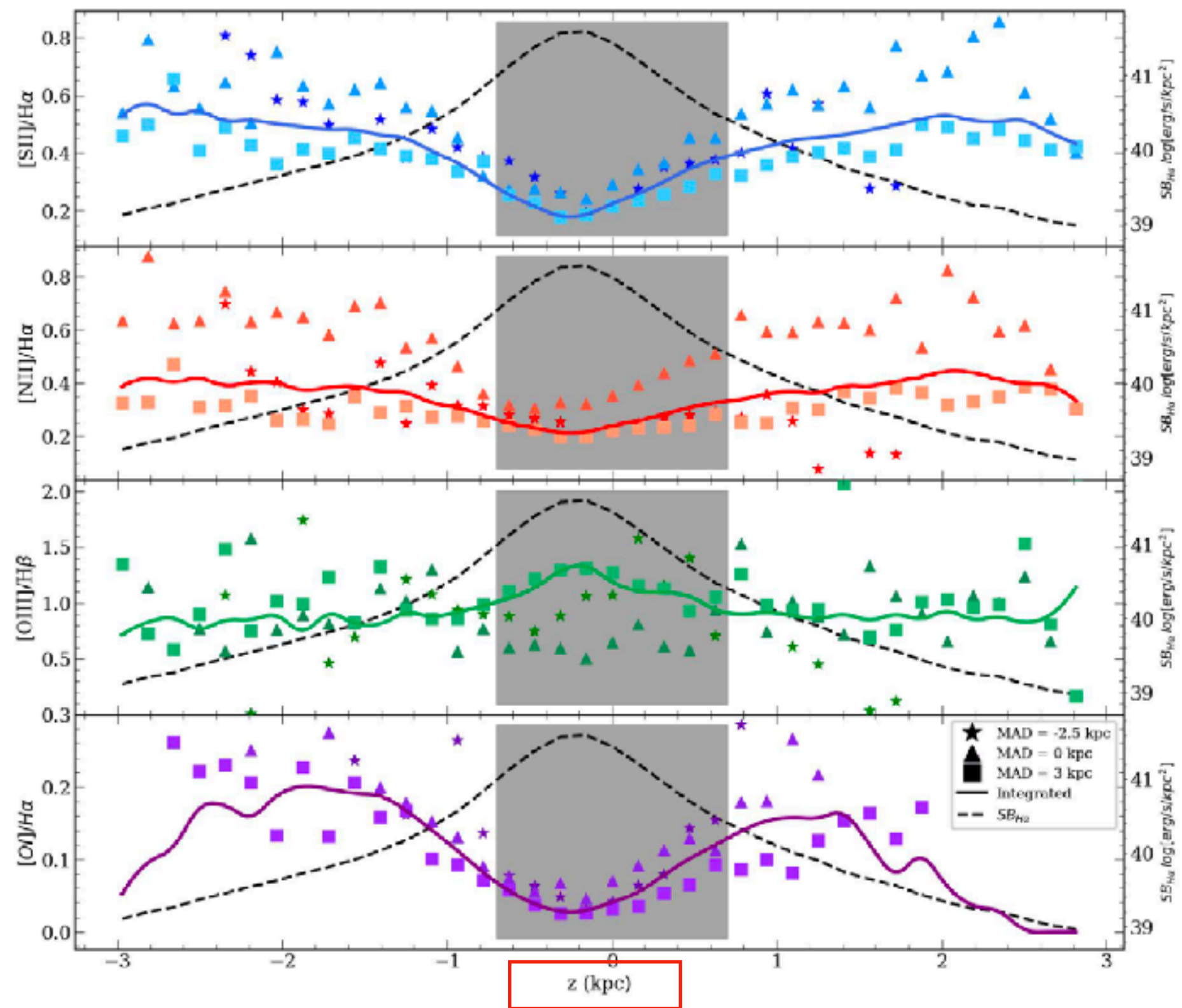
Fig. 3. Distribution of the line ratios with respect the distance from the midplane for the IC1553 galaxy. The star-shaped, triangular, and square markers represent the line ratio at that z for MAD = −2.5, 0, and 3 kpc, respectively, analogous to a long-slit perpendicular to the galactic plane at a given MAD. The solid lines represent the integrated values along the major axis distance. The dashed black line represents the $\Sigma_{H\alpha}$ height distribution of the galaxy. The grey background between $z = -0.7$ kpc and 0.7 kpc represents the galactic plane.

At MAD = 3 kpc (represented by squares in Figure 3, where the most prominent H II regions emission is observed in Figure 2), the [N II]/Hα, [S II]/Hα, and [O I]/Hα line distributions follow the same trend as their respective integrated distributions, but consistently reach lower values. Similarly, at MAD = 0 (represented by triangles in Figure 3, where the H II regions emission observed in Figure 2 is lower), the line distributions also follow the same trend, but consistently reach higher values. This

This behaviour in the line ratio distributions is consistent in all the galaxies, as shown in the appendices from A to H

Fig. 4. Major axis distance distribution of the [N II]/Hα and [S II]/Hα lines for IC1553 at $z = 1$ and 1.8 kpc. In green, the normalised $\Sigma_{H\alpha}$ MAD distribution, constructed by integrating the Hα flux within the ellipse fitted in Section 2 throughout the major axis. Both line distributions show a correspondence with the $\Sigma_{H\alpha}$ distribution, decreasing and showing a greater difference between the two heights as the $\Sigma_{H\alpha}$ increases. This tendency is consistent for all galaxies.

$\Sigma_{H\alpha}$ MAD distribution of IC1553. Two effects are noticeable in this figure: Firstly, all the line ratio distributions tend to be lower between 2 kpc and 4.5 kpc, where the $\Sigma_{H\alpha}$ is higher, and increase while the $\Sigma_{H\alpha}$ decreases, particularly for the [N II]/Hα ratio. Secondly, the effect of the increment of the line ratio with height, as seen in Figure 3, remains present along the major axis, with the difference being clearer in regions of high $\Sigma_{H\alpha}$, especially for the [S II]/Hα ratio, where there is a constant difference of 0.1 between both distributions. These effects are not exclusive

Связь между плоскостью и eDIG галактики

The correlation between the morphological distribution of star-forming regions in the discs of edge-on galaxies and the shapes and morphology of the halos presents the strongest evidence supporting the interpretation that energy sources from SF within the galaxy discs drive the observed disc-halo interactions

The specifics of the underlying mechanisms governing the disc-halo connection are complex and widely debated. From an energetic perspective, several external sources have been proposed to account for the origin of the eDIG.

?

However, in a recent study, Sardaneta et al. (2024) argue, based on a sample of nearby highly inclined (i ≥ 80), isolated galaxies, that the eDIG phenomenon is uncorrelated with the galaxy environment. Consequently, the primary energy sources driving the disc-halo interactions should reside within the galaxy discs, as no other pervasive external energy sources are known that could account for the observational data (Dahlem 1997). Therefore, the halo gas expelled or heated by these energy sources must also originate from the discs.

Связь между плоскостью и eDIG галактики

Several scenarios for the disc-halo interaction due to SF have been proposed:
- the superbubble breakout model (e.g. Mac Low & McCray 1988)
- the galactic fountain model (Shapiro & Field 1976),
- the champagne model (Tenorio-Tagle 1979)
- the chimney model (Norman & Ikeuchi 1989)
- the galactic wind model (Veilleux et al. 2005)

We exclude phenomena related to nuclear activity in galaxies or incoming gas from the IGM/CGM, and we focus on those models in which ionising radiation originating from SF must not only escape the H ii regions but also traverse the dense clouds of neutral hydrogen near the midplane.

In galaxies with intermediate SF levels, such as those in the eBETIS sample, disc-halo interactions occur only in regions with high SFR.

Furthermore, the detection of extended eDIG in the halos of the eBETIS sample indicates that even low-mass galaxies with modest SFR (Tables 1and 2) are capable of producing a pervasive layer of extraplanar diffuse ionised emission. This finding contradicts previous assumptions that halos are a rare phenomenon among normal spirals (Hummel et al. 1991), a bias likely caused by the insufficient sensitivity of earlier observations.
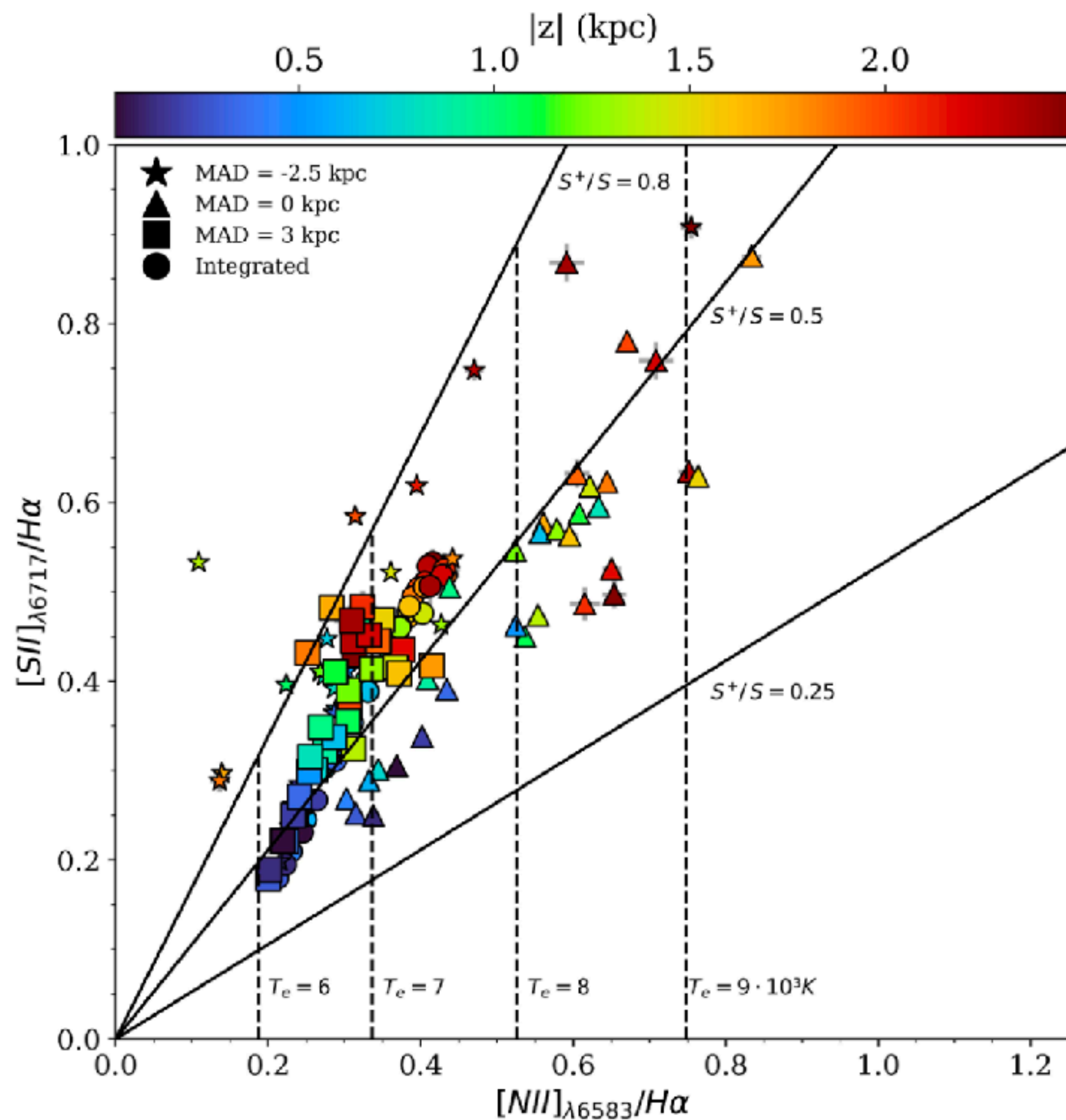
Механизмы ионизации eDIG

The precise underlying physics explaining the large distance between the extraplanar gas and ionising stars in the midplane, as well as the fine-tuned details of the ionisation mechanism of the eDIG, remain a topic of ongoing debate.

Long-standing issues regarding the specifics of OB-star-driven ionisation remain prevalent in the literature. A notable characteristic of the DIG that proves difficult to explain through OB star photoionisation is its optical emission-line spectrum.

Nonetheless, certain observed optical emission line ratios are not explicable by pure photoionisation from OB stars. The distinctive emission-line ratios observed in the eDIG, namely [N ii]λ6584/Hα, [S ii]λ6717/Hα, [O iii]λ5007/Hβ and [O i]λ6300/Hα, are elevated compared to those observed in H ii regions

Fig. 5. $[N\,\textsc{ii}]_{\lambda 6583}/H\alpha$ vs. $[S\,\textsc{ii}]_{\lambda 6717}/H\alpha$ diagnostic diagram for IC1553. Colours represent height with respect to the midplane, equally from above and below the plane. Vertical dashed lines are the theoretical ratios obtained from Eq. (1) at a constant T_e (6, 7, 8, and 9 in units of 10^3 K). Solid lines represent the theoretical ratios from Equations (1) and (2) for a fixed S^+/S (0.25, 0.5, and 0.8, respectively). The circles indicate the line ratios obtained by integrating the fluxes along the major axis at a certain z. Stars, triangles, and squares indicate the line ratio at a certain z for MAD $= -2.5$, 0, and 3 kpc, respectively.

Haffner et al. (1999) and Madsen et al. (2006) build diagnostic diagrams to estimate both Te and S+/S from observations of [N ii]/Hα and [S ii]/Hα

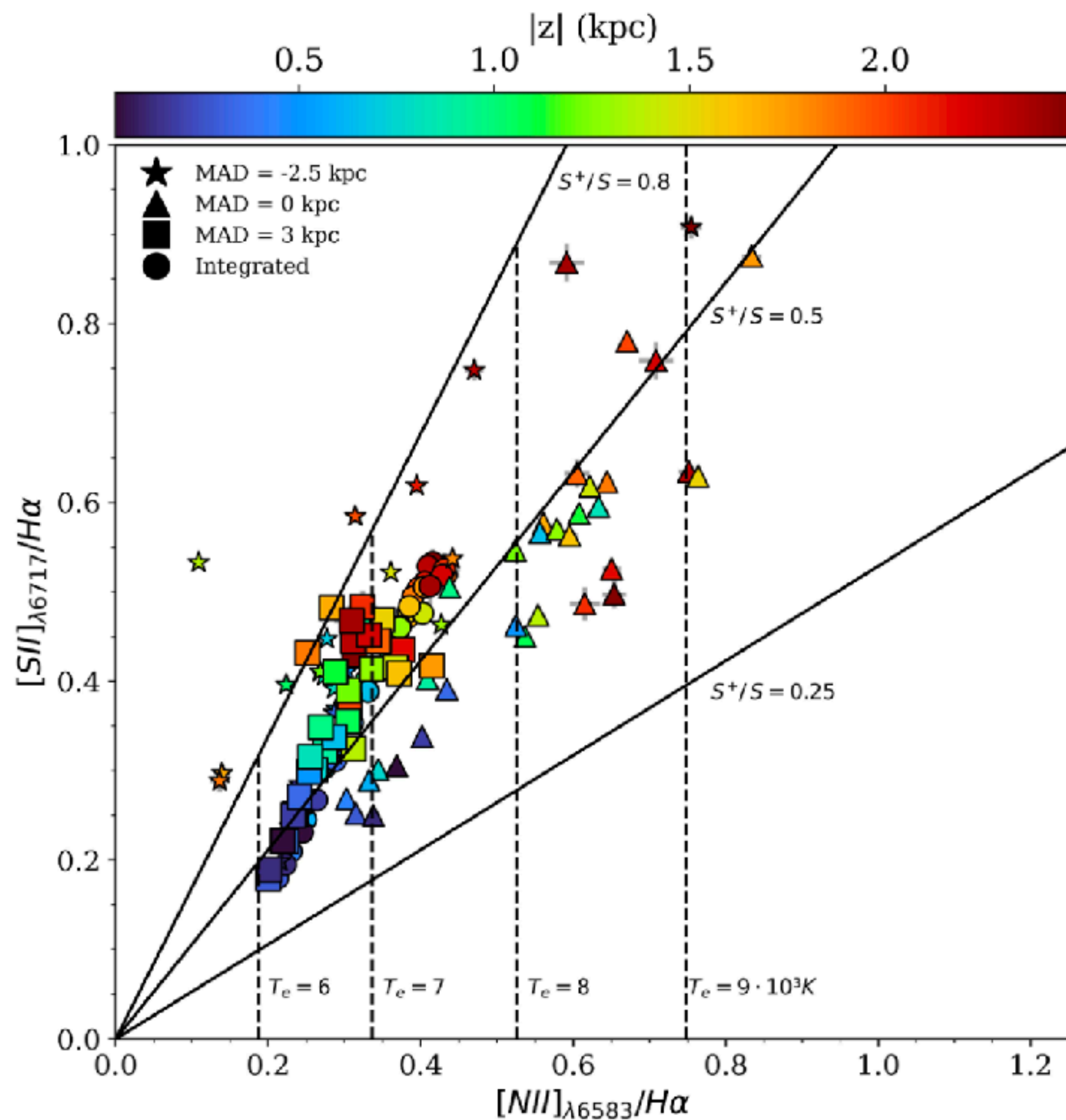Figure 5 illustrates significant variations in Te and S+/S with respect to the line of sight.

This provide more compelling evidence of the intricate dynamical heating structure of the ISM in the halo of late-type galaxies. A similar trend is observed across the entire eBETIS sample

The general behaviour indicates a linear, constant increment of Te with increasing distance from the galactic plane.

eDIG tends towards a lower ionisation state (higher S+/S~0.5–0.8) compared to classical H ii regions, which would be situated in the lower-left corner of these diagrams

Fig. 5. [N II]$_{\lambda 6583}$/Hα vs. [S II]$_{\lambda 6717}$/Hα diagnostic diagram for IC1553. Colours represent height with respect to the midplane, equally from above and below the plane. Vertical dashed lines are the theoretical ratios obtained from Eq. (1) at a constant T_e (6, 7, 8, and 9 in units of 10^3 K). Solid lines represent the theoretical ratios from Equations (1) and (2) for a fixed S$^+$/S (0.25, 0.5, and 0.8, respectively). The circles indicate the line ratios obtained by integrating the fluxes along the major axis at a certain z. Stars, triangles, and squares indicate the line ratio at a certain z for MAD $= -2.5$, 0, and 3 kpc, respectively.

The anomalous [N ii]/Hα and [S ii]/Hα eDIG line ratios can be attributed to an increase in the Te temperature in the halo, resulting from photoionisation with a low ionisation parameter q (i.e. the ratio of ionising photon density to electron density, which measures the diluteness of the radiation field). But other eDIG line ratios, such as [O iii]/Hβ and [O i]/Hα, remain unexplained

What remains puzzling in this scenario is the increase in Te with respect to |z|. The observed temperature behaviour of the eDIG could be attributed to the spectrum of the ionising radiation being reprocessed as it traverses the ISM, an effect known as radiation hardening.

But this model fails to explain an increasing [O iii]/Hβ ratio at large distances from the galactic plane. Therefore, the rise in the [O iii] ratio with H-recombination lines with |z| needs an additional source of heating and/or ionisation.

Механизмы ионизации eDIG

Дальше достаточно подробно рассказывается про гипотезу, где вторичным источником ионизации являются HOLMES, про все достоинства этой гипотезы, но:

Nevertheless, the behaviour of the line ratios shown reveals that the ionisation of the eDIG is highly dependent on the distribution of H ii regions in the disc. The [N ii]/Hα, [S ii]/Hα, and [O iii]/Hβ ratios attain their highest values at the greatest distances from the midplane and in regions with lower ΣHα. This correlation between the ionisation structure of the eDIG and the H ii region distribution observed in this study does not support a homogeneous distribution of HOLMES across the thick disc and lower halo.

This observation is incompatible with a smooth distribution of HOLMES throughout the thick disc and lower halo. Under the HOLMES scenario, higher [O iii]/Hβ ratios would be expected in the vicinities of the thick disc, along with a smooth distribution of characteristic high ionisation line ratios within the halos. Furthermore, the few high [O iii]/Hβ ratio bins near the galactic planes of the galaxies are clearly associated with SF regions within the discs. Then, the behaviour of the [N ii]/Hα, [S ii]/Hα, and [O iii]/Hβ ratios alone is not sufficient evidence to conclusively support HOLMES as an ionisation source.

Механизмы ионизации eDIG

Далее подробно рассказывается о гипотезе, связанной с ударными волнами, их происхождении на больших высотах и плюсах данной гипотезы для описания eDIG и, в частности, для объяснения поведения [O iii]/Hβ

Interfaces between hot (10^6 K) and cooler(≤10^4 K) gas are prevalent throughout the ISM at significant z distances from the galaxies' midplanes. The gas at intermediate temperatures of ~10^5 K at these interfaces generates extreme ultraviolet (EUV) ionising radiation. The radiation of these hot-cool gas interfaces in the halo may constitute a significant source of ionising radiation for distant clouds and regions where LyC ionising radiation from OB stars in the midplane is eithershielded or absent.

Shocks induced in the ISM by feedback mechanisms, such as supersonic winds originating from high-level SF regions, have been proposed as a significant source of heating for the eDIG

Given that shock heating is significant only if the kinetic energy is efficiently thermalised, both photoionisation and shocks can be regarded as "thermal" heating sources of the ISM. Crucially, the observed rising trend in the [O iii]/Hβ emission line ratio with height can be expected as a mixing sequence between the predominant shock ionisation in the halo and photoionisation in the disc. Shocks therefore emerge as the most promising secondary ionisation mechanism for the eDIG.

Механизмы ионизации eDIG

Далее подробно рассказывается о гипотезе, связанной с ударными волнами, их происхождении на больших высотах и плюсах данной гипотезы для описания eDIG и, в частности, для объяснения поведения [O iii]/Hβ

Interfaces between hot (10^6 K) and cooler(≤10^4 K) gas are prevalent throughout the ISM at significant z distances from the galaxies' midplanes. The gas at intermediate temperatures of ~10^5 K at these interfaces generates extreme ultraviolet (EUV) ionising radiation. The radiation of these hot-cool gas interfaces in the halo may constitute a significant source of ionising radiation for distant clouds and regions where LyC ionising radiation from OB stars in the midplane is eithershielded or absent.

Shocks induced in the ISM by feedback mechanisms, such as supersonic winds originating from high-level SF regions, have been proposed as a significant source of heating for the eDIG

Given that shoc... ...otoionisation
and shocks can ... trend in the
[O iii]/Hβ emiss... ...minant shock
ionisation in the... ...sing secondary
ionisation mech...

[4] We note that tidal interactions and AGN jets can also produce shock ionisation in the halos of galaxies, with similar effects as discussed in the text (e.g. Dopita & Sutherland 1995; Simpson et al. 2007; Rich et al. 2011; Ho et al. 2016; Molina et al. 2018).
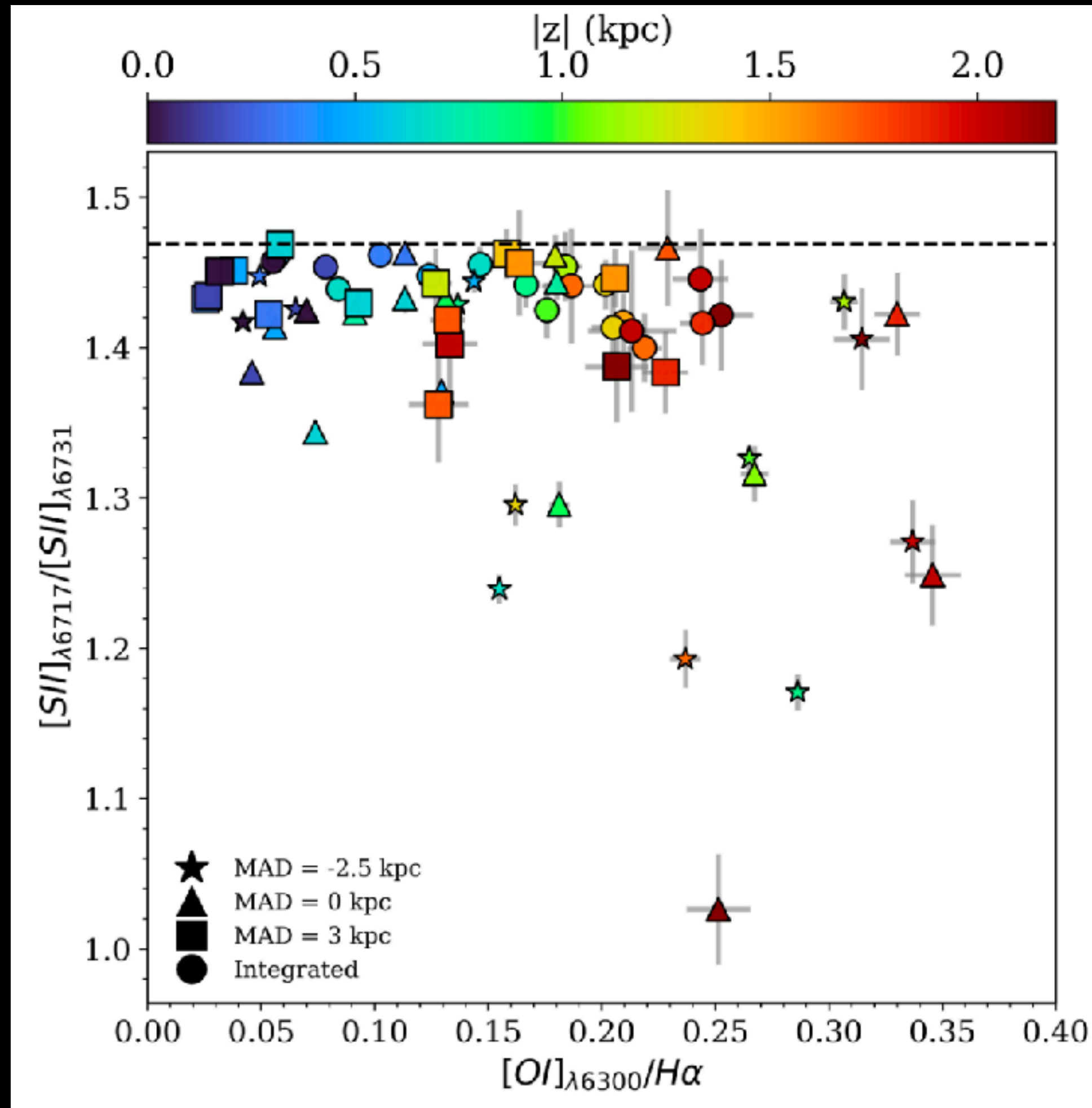
The top-panel of Figure 8 shows the observed $[S\,II]_{\lambda6717}/[S\,II]_{\lambda6731}$ doublet ratio versus the $[O\,I]_{\lambda6300}/H\alpha$ line ratio for various binned sections in the halo of IC1553 at different galactocentric distances. The $[S\,II]$ doublet is employed to infer the electron gas density; this ratio diminishes as the electron gas density increases, with a low-density limit of approximately 1.5, corresponding to an electron density of $n_e \leq 10\,cm^{-3}$ (Osterbrock & Ferland 2006). Most of the eDIG regions near the midplane of IC1553 exhibit $[S\,II]$ line ratios close to this low-density limit, accompanied by low $[O\,I]/H\alpha$ values, indicative of $H\,II$ region emission. However, for bins corresponding to a higher altitude $|z|$ from the midplane, the $[S\,II]_{\lambda6717}/[S\,II]_{\lambda6731}$ ratio decreases to values between 1.0 and 1.3, implying high electron densities in the range of $n_e \sim 200-800\,cm^{-3}$.

The most striking feature of this figure is that the regions with low $[S\,II]$ doublet ratios coincide with regions exhibiting high $[O\,I]/H\alpha$ values (>0.25), indicative of shock-compressed ionised gas. Therefore, the low doublet $[S\,II]$ ratios, their implied high gas density, and the fact that these regions exhibit higher $[O\,I]/H\alpha$ values are consistent with a scenario wherein gas emission originates from shocks, likely induced by feedback from high-level SF regions within the galactic disc. In this scenario,

Hybrid SF and shock ionisation mechanism of the eDIG
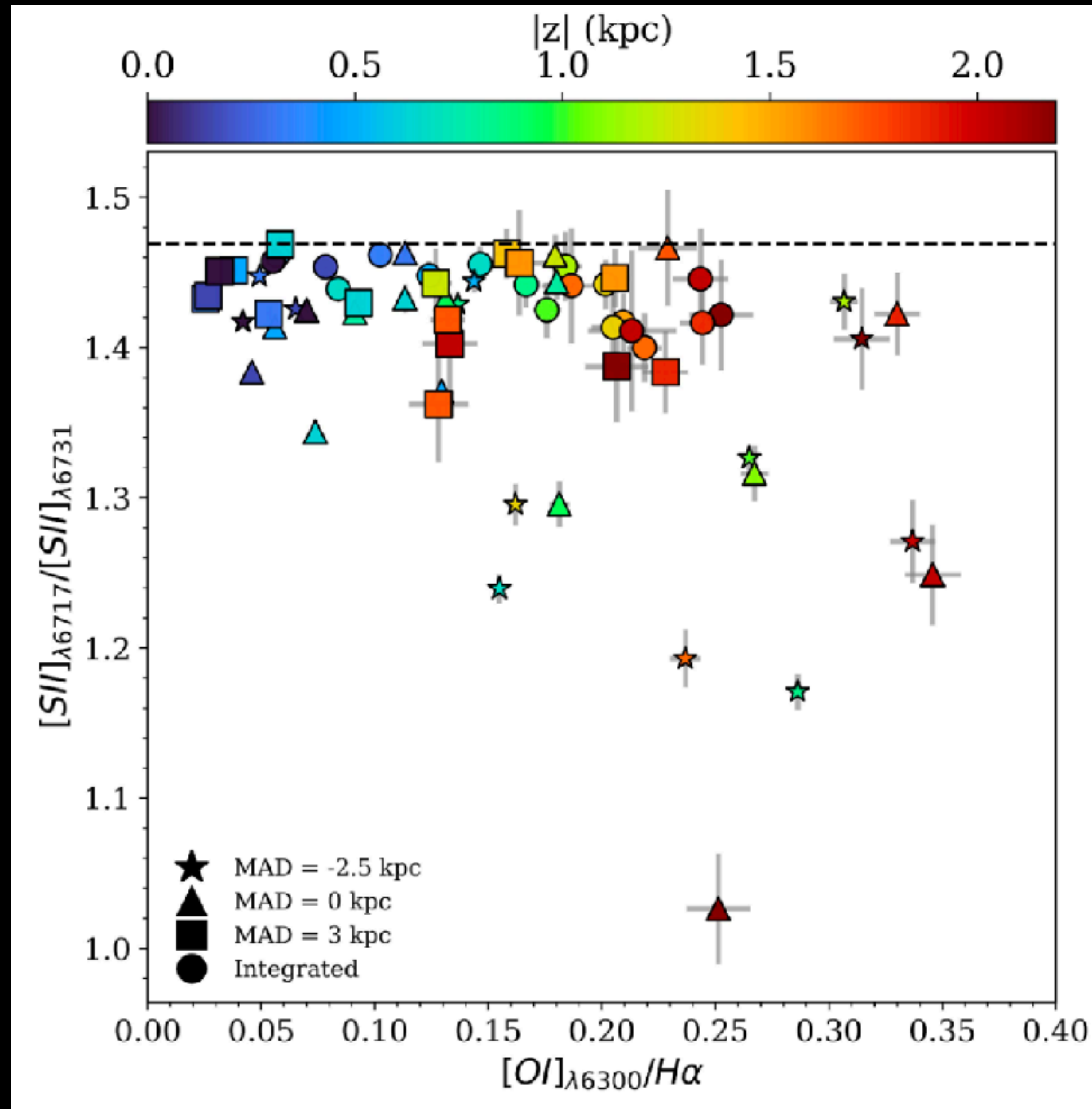
the galactic disc. In this scenario, fast shocks can account for the increase in the [O I]/Hα ratio with distance from the midplane, with the highest [O I]/Hα ratios corresponding to the shocked interface at the greatest distances from the midplane.
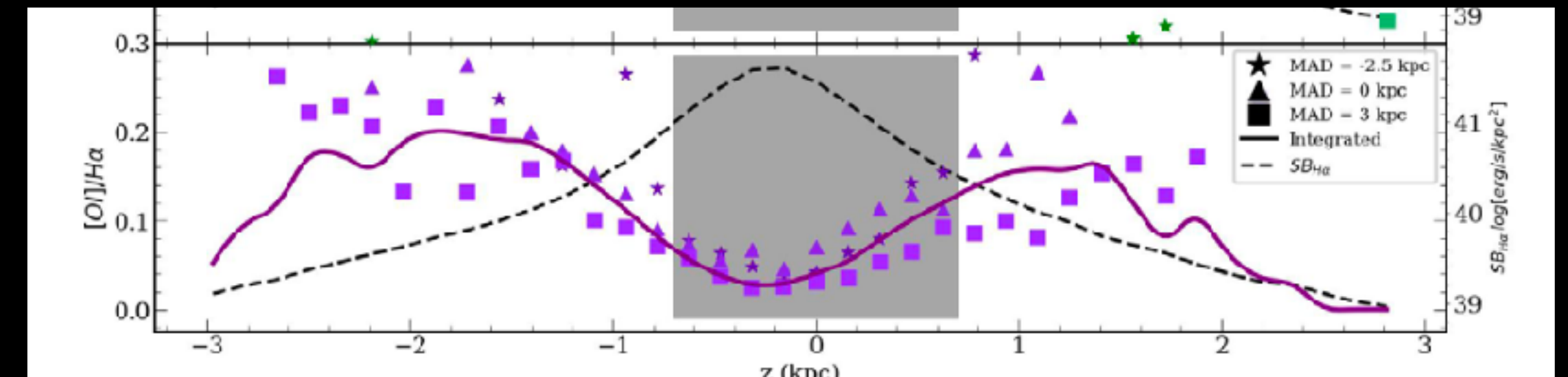
Hybrid SF and shock ionisation mechanism of the eDIG

Thus, we explore the combination of photoionisation from H ii regions and ionisation due to fast shocks as simultaneous contributors to the ionisation mechanism of the eDIG. This is achieved by constructing a set of hybrid models that incorporate both star formation and fast shock mechanisms.

We firstly consider the photoionisation models for low-metallicity star-forming galaxies of Levesque et al. (2010). The grids of this models predict the line ratios involved in the typical BPT diagram (Baldwin et al. 1981) for a pure photoionisation regime due to the star formation with ionisation parameters (q) ranging from 10^7 to 2×10^8 cm/s and metallicities (Z) from 0.001

to 0.04. Each model grid is computed for electron densities n_e of 10, 10^2, 10^3 and 10^4 cm^{-3}, assuming either continuous star formation or an instantaneous burst of star formation at 0 Myr.

On the other hand, we consider the fast shocks models of Allen et al. (2008). This models predict the flux of the ionising radiation produced by a shock. The flux is dependent on the shock velocity ($f \propto v_s^3$). Therefore, if the shock velocity surpasses the velocity of the photoionisation front (in the case of a low ionisation parameter), the ionising photons are absorbed by the surrounding gas, altering its ionisation state. In another scenario, if $v_s \approx 170$ km/s, the ionisation front velocity now exceed the velocity of the shock, pre-ionising the surrounding gas and changing the optical emission lines observed (McKee & Hollenbach 1980). The fast shocks models of Allen et al. (2008) consider this two scenarios, with preshock densities ranging from 0.01 to 1000 cm^{-3}, shock velocities from 100 to 1000 km/s and magnetic field ($B/n^{1/2}$) from 10^{-4} to 100 μG cm$^{3/2}$.
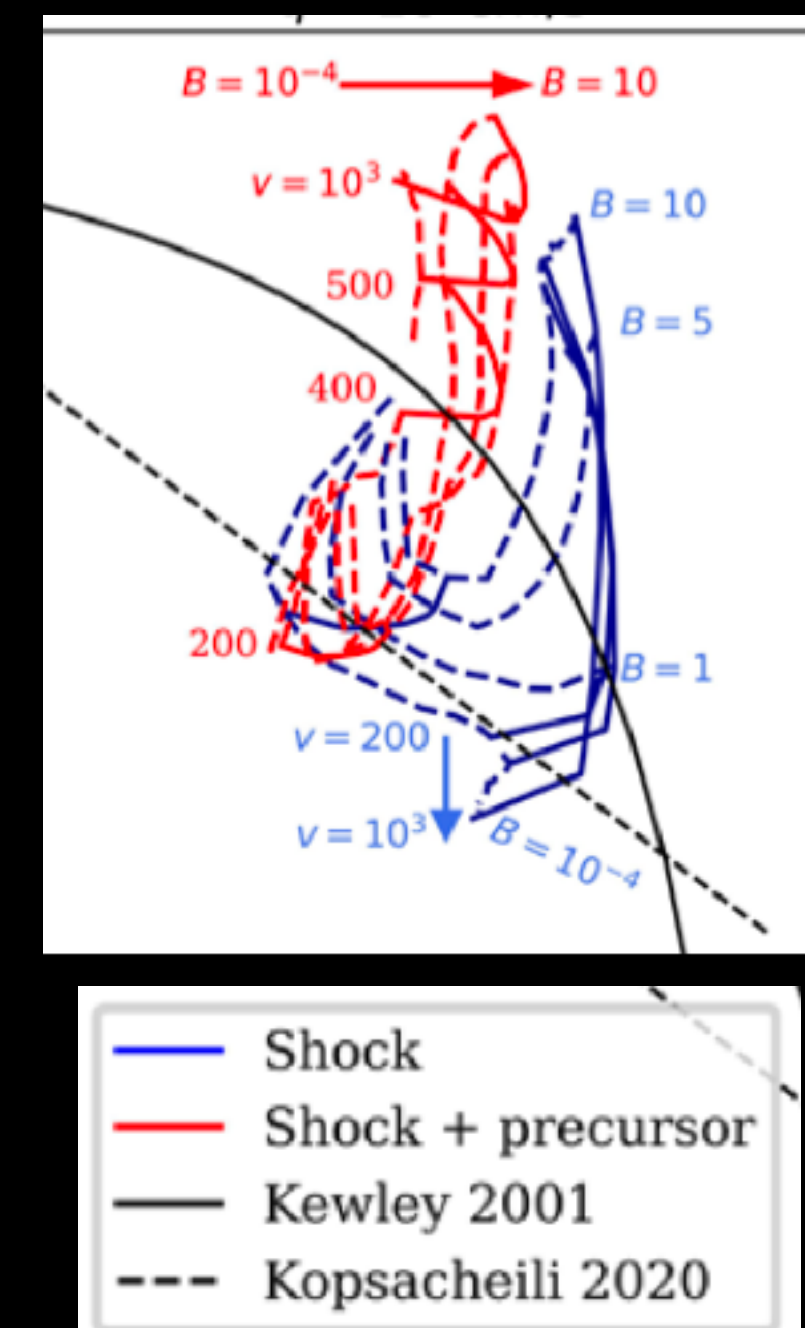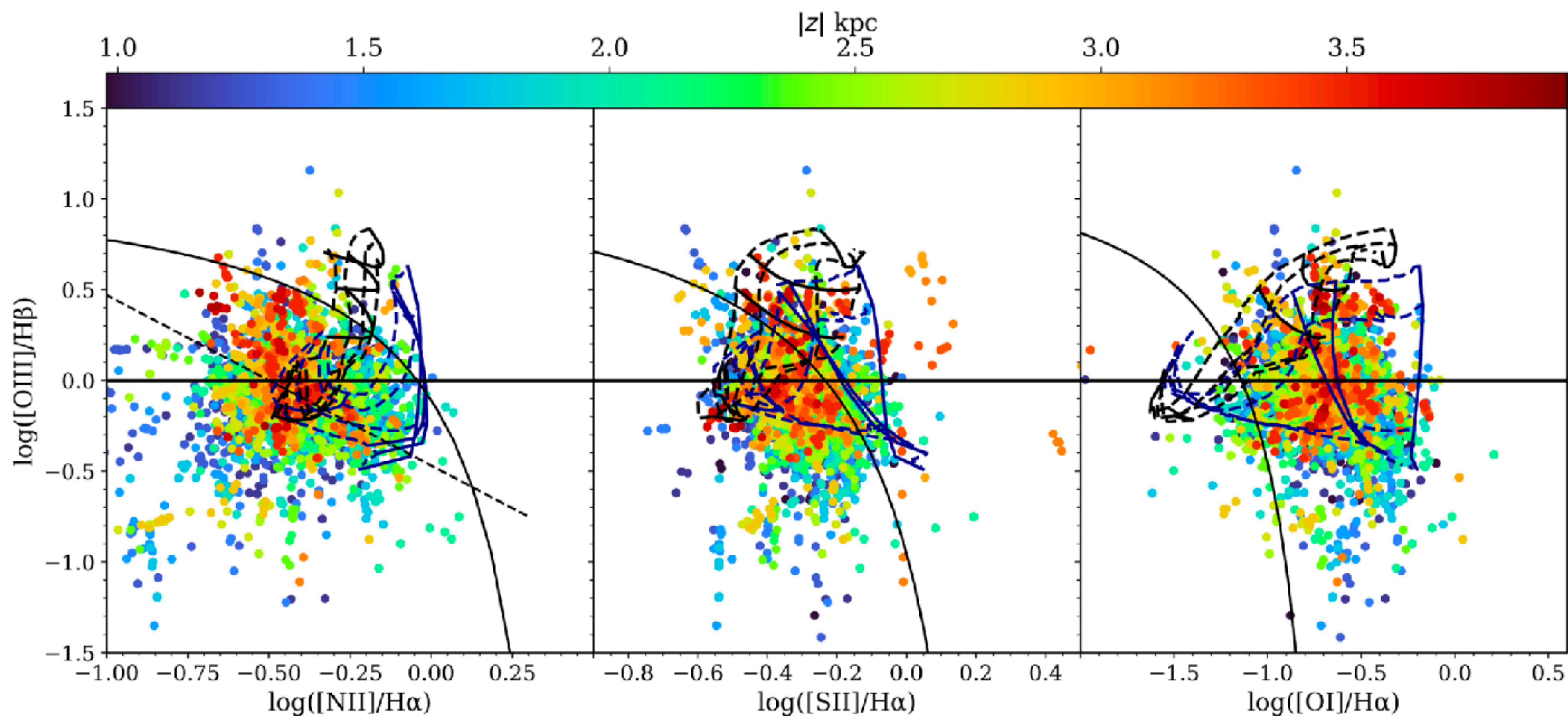
Hybrid SF and shock ionisation mechanism of the eDIG

Thus, we explore the combination of photoionisation from H ii regions and ionisation due to fast shocks as simultaneous contributors to the ionisation mechanism of the eDIG. This is achieved by constructing a set of hybrid models that incorporate both star formation and fast shock mechanisms.

Our hybrid models are constructed as follows: we consider both shock models, with and without assuming pre-ionisation. Then, for each shock model, we assume that the predicted flux corresponding to shock wind velocity of 200, 400, 500 and 1000 km/s and magnetic field of 10^{-4}, 1.0, 5.0 and $10\,\mu G\,cm^{3/2}$ contributes only a fraction $f_{shock} \in [0, 1]$ of the total observed ionising flux. The remaining fraction $1 - f_{shock}$ corresponds to the flux predicted by a grid model with a certain ionisation parameter and metallicity from Levesque et al. (2010).
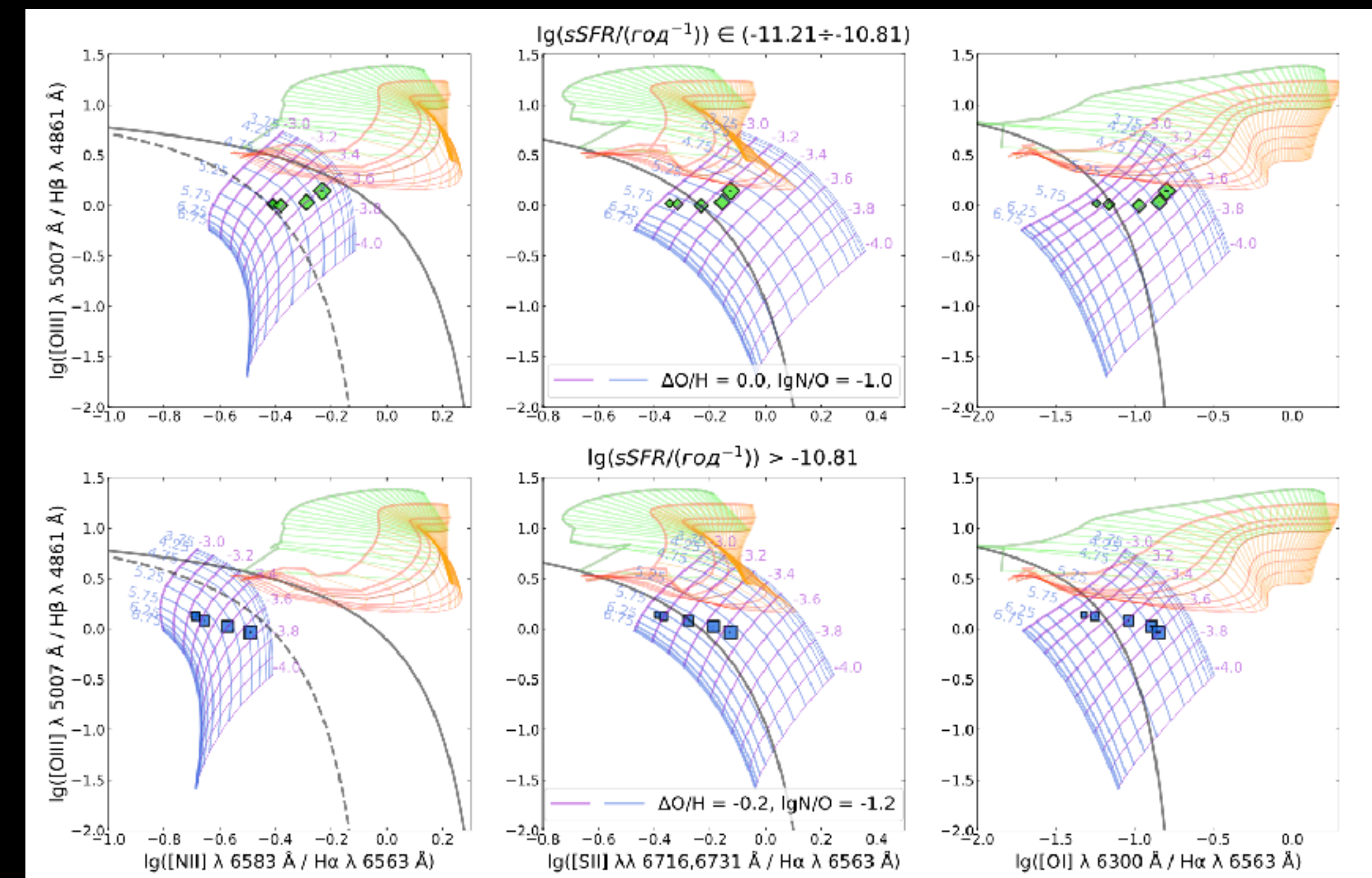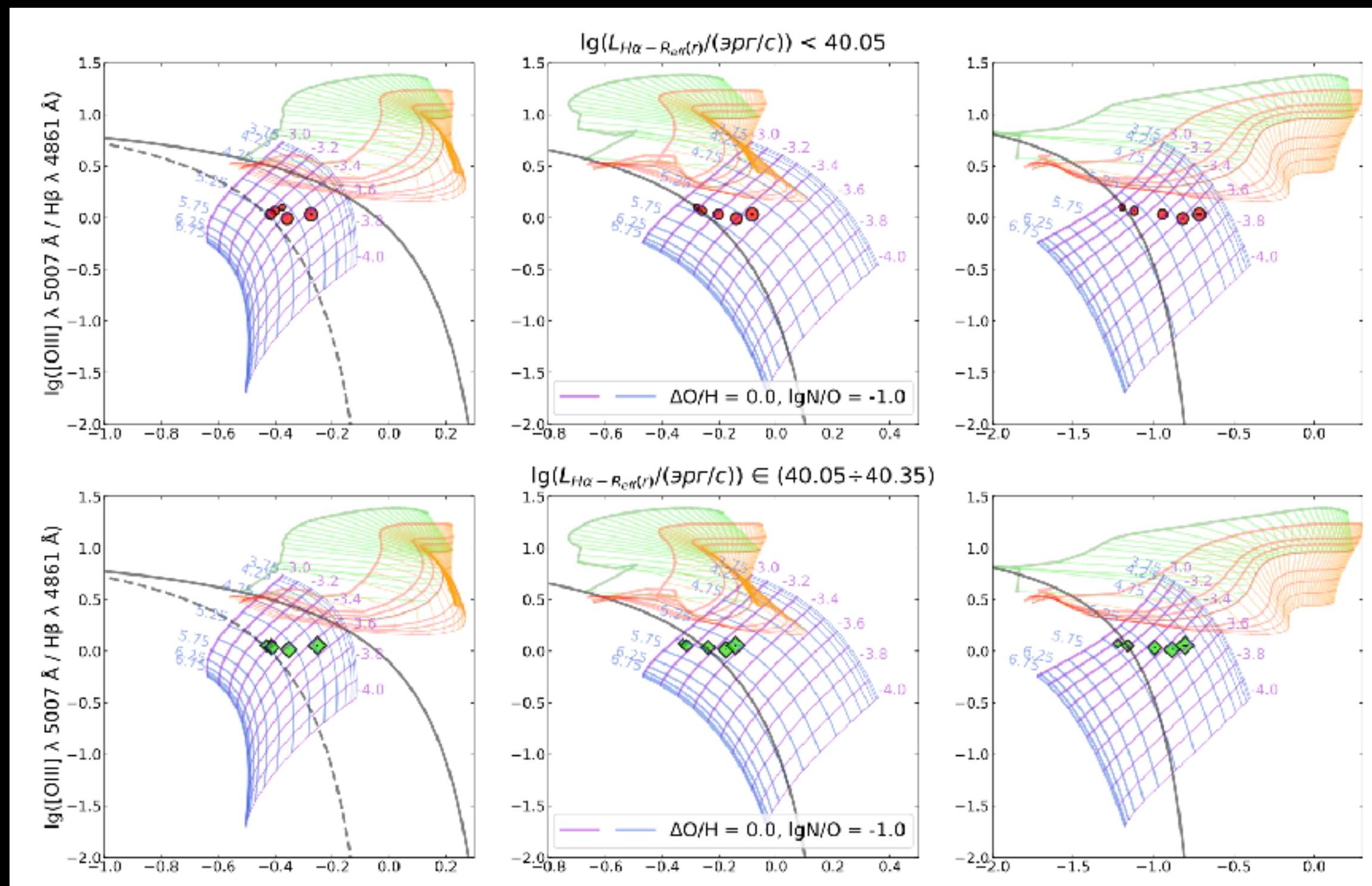
Hybrid SF and shock ionisation mechanism of the eDIG

Fig. 7. BPT for all eDIG bins of IC1553, with the colours coding the vertical distance (both above and below) from the midplane. The plotted hybrid models correspond to 40% of the flux due to fast shocks with preionisation (curves lines) and with front shock only (blue curves), and 60% of the flux due to star formation with $Z = Z_\odot$ and $q = 10^7$ cm/s. Solid curves correspond to the shock winds from 200 to 1000 km/s, and dashed curves represent magnetic field intensities from 0.0001 to 10 μG cm$^{3/2}$. The Kopsacheili et al. (2020) and Kewley et al. (2001) lines are also plotted, as in Figure 6.
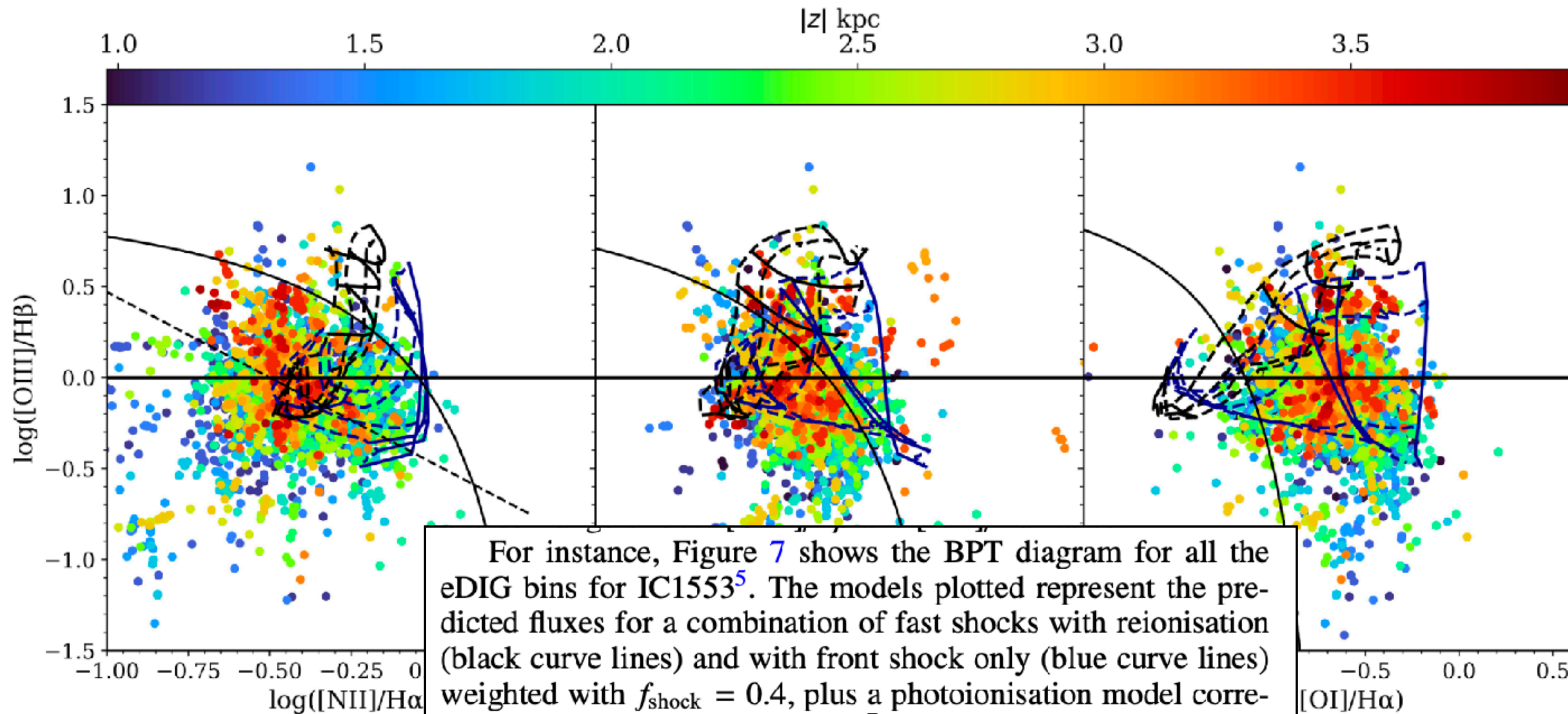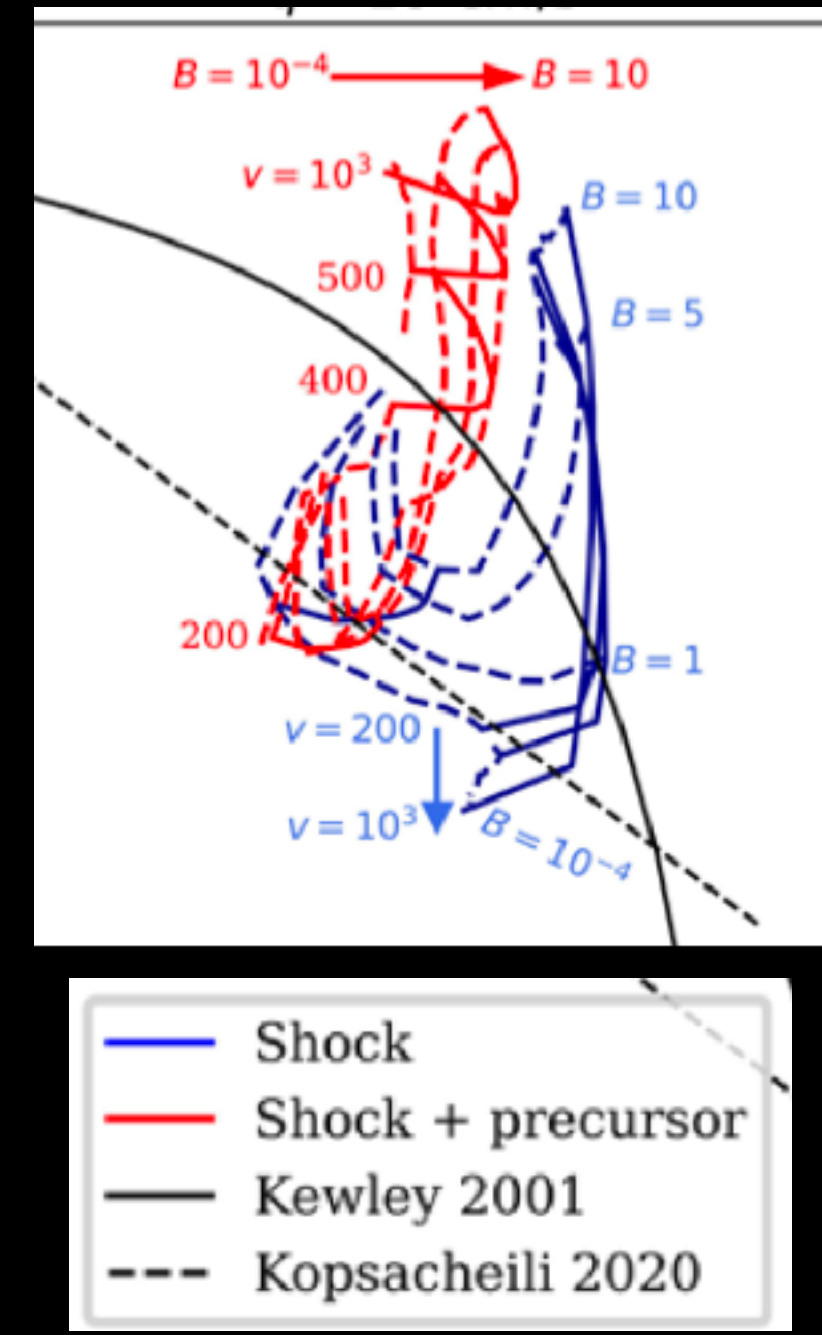
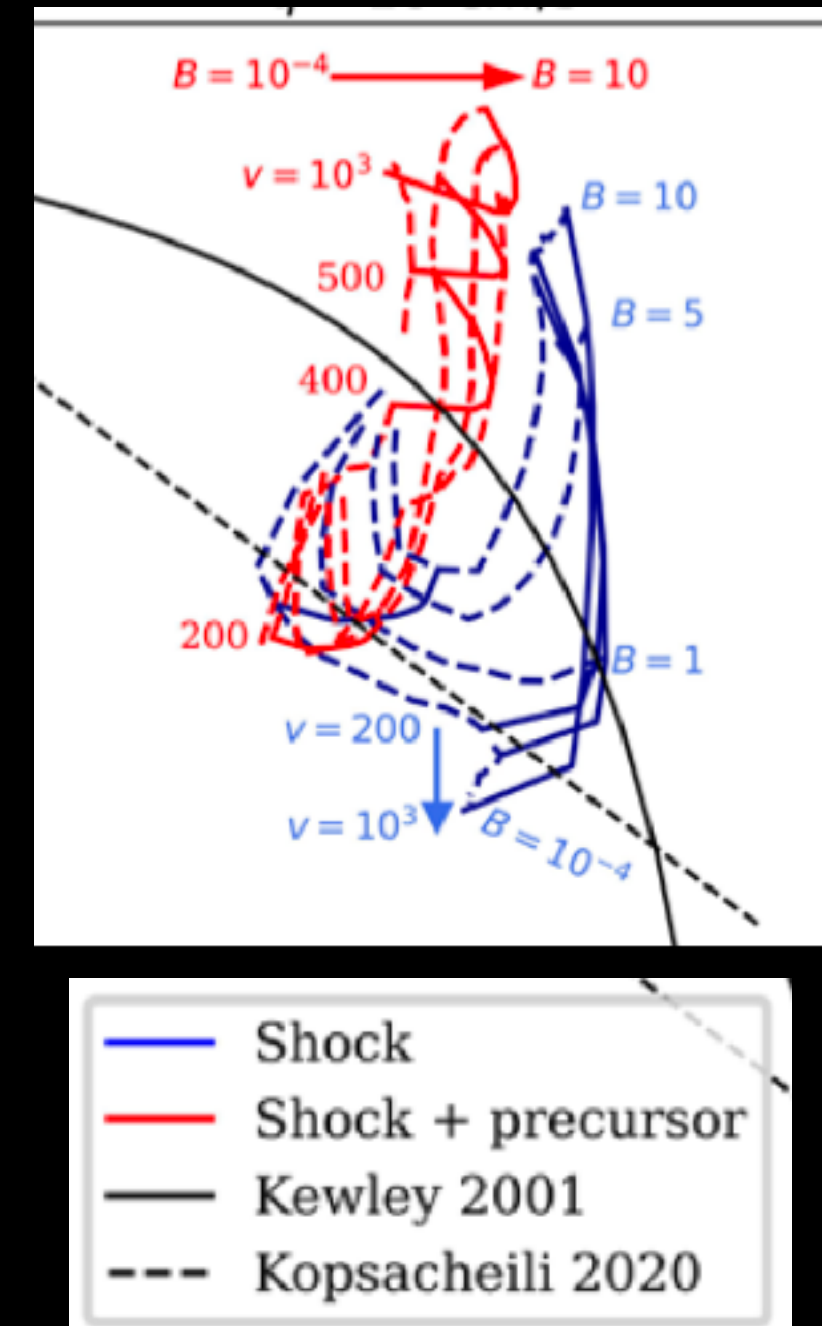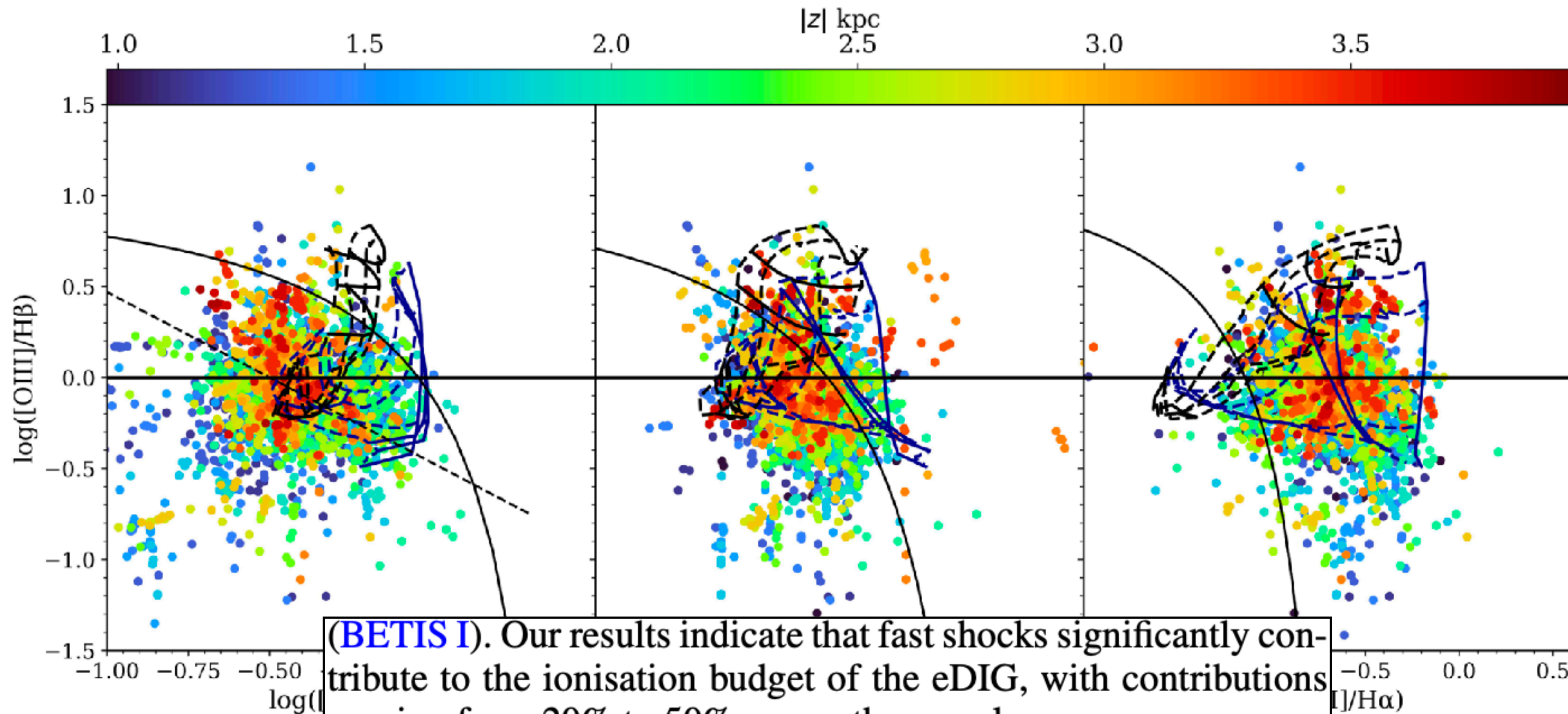# Hybrid SF and shock ionisation mechanism of the eDIG

For instance, Figure 7 shows the BPT diagram for all the eDIG bins for IC1553[5]. The models plotted represent the predicted fluxes for a combination of fast shocks with reionisation (black curve lines) and with front shock only (blue curve lines) weighted with $f_{shock} = 0.4$, plus a photoionisation model correspondent to $Z = Z_\odot$ and $q = 10^7$ cm/s, for instantaneous burst at 0 Myr and $n_e = 100\,\mathrm{cm^{-3}}$. Thus, the fluxes predicted for

Fig. 7. BPT for all eDIG bins of IC1553[...] in the midplane. The plotted hybrid models correspond to 40% of the flux due to fast shocks with preionisation (curves lines) and with front shock only (blue curves), and 60% of the flux due to star formation with $Z = Z_\odot$ and $q = 10^7$ cm/s. Solid curves correspond to the shock winds from 200 to 1000 km/s, and dashed curves represent magnetic field intensities from 0.0001 to 10 μG cm$^{3/2}$. The Kopsacheili et al. (2020) and Kewley et al. (2001) lines are also plotted, as in Figure 6.

Hybrid SF and shock ionisation mechanism of the eDIG

(BETIS I). Our results indicate that fast shocks significantly contribute to the ionisation budget of the eDIG, with contributions ranging from 20% to 50% across the sample.

Fig. 7. BPT for all eDIG bins of IC1553, with the colours coding the vertical distance (both above and below) from the midplane. The plotted hybrid models correspond to 40% of the flux due to fast shocks with preionisation (curves lines) and with front shock only (blue curves), and 60% of the flux due to star formation with $Z = Z_\odot$ and $q = 10^7$ cm/s. Solid curves correspond to the shock winds from 200 to 1000 km/s, and dashed curves represent magnetic field intensities from 0.0001 to 10 μG cm$^{3/2}$. The Kopsacheili et al. (2020) and Kewley et al. (2001) lines are also plotted, as in Figure 6.
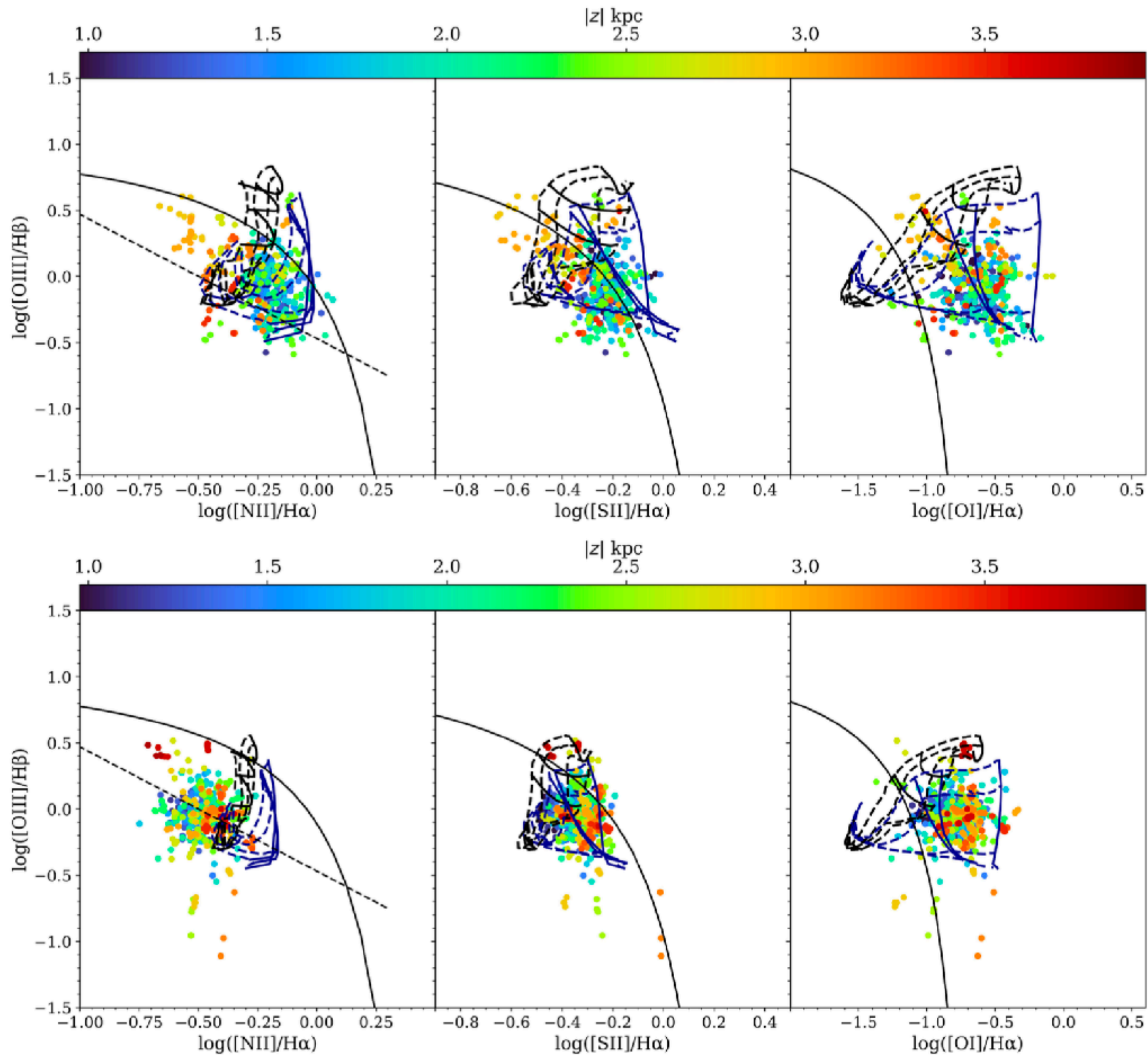
Fig. 10. IC1553 BPT with hybrid models, similar to Figure 7. Top: eDIG bins corresponding to the biconical structure seen in the [N II]/Hα map, within −0.5 kpc < MAD < 0.5 kpc. The hybrid models that best fit the data correspond to 40% shocks and 60% SF with $Z = Z_\odot$ and $q = 10^7$ cm/s. Bottom: eDIG bins corresponding to the high-SF feature on the southern edge of the disc, within 2.5 kpc < MAD < 3.5 kpc. The hybrid models that best fit the data correspond to 20% shocks and 80% SF with $Z = Z_\odot$ and $q = 10^7$ cm/s.
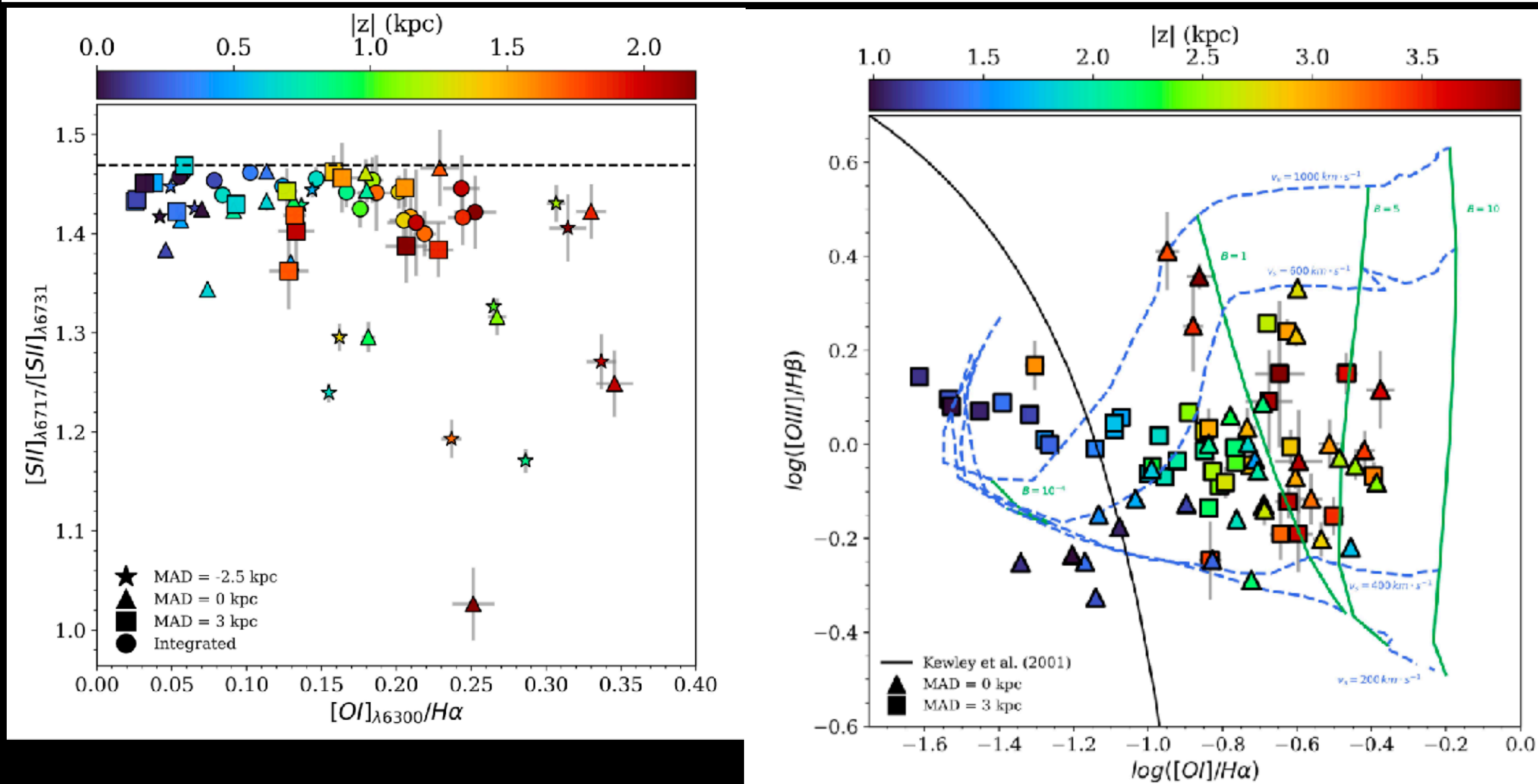
The contribution of fast shocks can vary significantly across different regions of the halo, with variations reaching up to 20% within the same galaxy. This variability arises from the distinct properties, physical processes, and structures inherent to each galaxy that affect the ionisation of the extraplanar gas. These structures include filaments, knots, extraplanar H II regions, and nearby neighbouring galaxies. Nonetheless, the distribution of H II regions within the disc consistently exerts a substantial influence on the ionisation of the halo gas.

Hybrid SF and shock ionisation mechanism of the eDIG

Fig. 8. [O I]/Hα vs. line ratios. Top: Electron-density-sensitive [S II]$_{\lambda6717}$/[S II]$_{\lambda6731}$ line ratio vs. shocks-proxy [O I]$_{\lambda6300}$/Hα line ratio for IC1553. The dashed horizontal line represents the theoretical low-density limit for the [S II] doublet, corresponding to 1.469 (Osterbrock & Ferland 2006). Colours and symbols are the same as in Figure 5. Bottom: [O III]/Hβ vs. [O I]/Hα diagnostic diagram for the bins of IC1553 at the minor axis, centred in the biconical structure seen in the [N II]/Hα map (triangles) and in the region within 2.5 < MAD < 4.5 kpc (squares), coincident with the high-level SF region visible in the disc of the galaxy. Curves represent the hybrid model for 40% shocks (without precursor) and 60% star formation with $Z = Z_\odot$ and $q = 10^7$ cm/s.

The top-panel of Figure 8 shows the observed [S II]$_{\lambda6717}$/[S II]$_{\lambda6731}$ doublet ratio versus the [O I]$_{\lambda6300}$/Hα line ratio for various binned sections in the halo of IC1553 at different galactocentric distances. The [S II] doublet is employed to infer the electron gas density; this ratio diminishes as the electron gas density increases, with a low-density limit of approximately 1.5, corresponding to an electron density of $n_e \leq 10\,\mathrm{cm}^{-3}$ (Osterbrock & Ferland 2006). Most of the eDIG regions near the midplane of IC1553 exhibit [S II] line ratios close to this low-density limit, accompanied by low [O I]/Hα values, indicative of H II region emission. However, for bins corresponding to a higher altitude |z| from the midplane, the [S II]$_{\lambda6717}$/[S II]$_{\lambda6731}$ ratio decreases to values between 1.0 and 1.3, implying high electron densities in the range of $n_e \sim 200–800\,\mathrm{cm}^{-3}$.

the presence of shock excitation. Consequently, a model incorporating star-forming ionisation with shock ionisation as an additional heating source offers the most satisfactory explanation for the relatively high [O I]/Hα and [O III]/Hβ ratios observed in the lowest surface brightness regions as a function of distance from the midplane in edge-on star-forming galaxies.